scientific reports

Check for updates

OPEN

Robust and reproducible human intestinal organoid-derived monolayer model for analyzing drug absorption

Kai Tanaka[1]✉, Tatsuki Mochizuki[1], Shogo Baba[2], Shigeto Kawai[1], Kiyotaka Nakano[1], Tatsuhiko Tachibana[1], Kohsuke Uchimura[1], Atsuhiko Kato[1], Takashi Miyayama[1], Tomohito Yamaguchi[3], Hiroshi Nishihara[4], Kimio Terao[5] & Yasutaka Kato[2,4]

Predicting the absorption of orally administered drugs is crucial to drug development. Current in vitro models lack physiological relevance, robustness, and reproducibility, thus hindering reliable predictions. In this study, we developed a reproducible and robust culture method to generate a human intestinal organoid-derived monolayer model that can be applied to study drug absorption through a step-by-step approach. Our model showed similarity to primary enterocytes in terms of the drug absorption-related gene expression profile, tight barrier function, tolerability toward artificial bile juice, drug transporter and metabolizing enzyme function, and nuclear receptor activity. This method can be applied to organoids derived from multiple donors. The permeability of launched 19 drugs in our model demonstrated a correlation with human Fa values, with an R^2 value of 0.88. Additionally, by combining the modeling and simulation approaches, the estimated FaFg values for seven out of nine drugs, including CYP3A substrates, fell within 1.5 times the range of the human FaFg values. Applying this method to the drug discovery process might bridge the gap between preclinical and clinical research and increase the success rates of drug development.

Keywords Drug absorption modeling, Human intestinal organoids, Pharmacokinetic prediction, In vitro drug screening, Precision drug development

The oral route of drug administration is commonly used in pharmacotherapy owing to its low invasiveness, improved drug adherence, and cost effectiveness. The small intestine is the primary site of most drug absorption. The intestinal epithelium forms a physical barrier via tight cell–cell adhesion and a mucus layer comprising cells such as MUC2 protein-producing goblet cells, actively excretes xenobiotics through drug efflux transporters such as P-glycoprotein (P-gp) and breast cancer resistant protein (BCRP), and degrades them through drug-metabolizing enzymes such as cytochrome P450 3A4 (CYP3A4), which accounts for 30% of drug metabolism in humans[1]. Nuclear receptors regulate the expression of these transporters and metabolizing enzymes. Some commercial drugs are substrates for nuclear receptors, causing drug–drug interactions. Therefore, evaluating the impact of drug candidates on these key factors and predicting the fraction absorbed from the gut lumen to enterocytes (fraction absorbed, Fa), first-pass metabolism in the intestine (intestinal availability, Fg), and the fraction of the dose absorbed into the portal blood after oral administration (Fa × Fg) are essential steps in drug development. Drug absorption in humans is frequently predicted using animals; however, they are not always suitable because of species differences[2,3].

In vitro models have been constructed to gain insights into the complex drug absorption processes. A human colon adenocarcinoma cell line Caco-2 model is commonly utilized for predicting drug absorption[4,5]. This model is useful with respect to several points; however, it lacks drug metabolizing enzymes and nuclear receptor function[6]. Recently, protocols have been modified to induce induced pluripotent stem cell-derived

[1]Translational Research Division, Chugai Pharmaceutical Co., Ltd, 216 Totsuka Totsuka-Ku Yokohama, Kanagawa, Japan. [2]Department of Biology and Genetics, Laboratory of Cancer Medical Science, Hokuto Hospital, 7-5 Kisen, Inadacho, Obihiro, Hokkaido, Japan. [3]Department of Gastroenterology, Hokuto Hospital, 7-5 Kisen, Inadacho, Obihiro, Hokkaido, Japan. [4]Keio Cancer Center, Keio University School of Medicine, 35 Shinanomachi, Shinjuku-Ku, Tokyo, Japan. [5]Translational Research Division, Chugai Pharmaceutical Co., Ltd, 2-1-1 Nihonbashi-Muromachi Chuo-Ku, Tokyo, Japan. ✉email: tanaka.kai11@chugai-pharm.co.jp

enterocyte-like cells to emulate absorption process in humans[7–10]. Although remarkable progress has been achieved, there are still challenges with the maturation status of cells compared to in vivo. The other approach is to utilize adult stem cell-derived organoids[11–14]. Organoids can be differentiated into mature intestinal cells, that retain the characteristics of the original intestinal tissue region[13,15–20]. Researchers have developed several monolayer culture models using intestinal organoids to assess drug absorption[21–25]. Notably, Michiba et al. used a monolayer model to predict Fg values with superior predictive accuracy[24]. Despite these advancements, in vitro models using organoids face challenges in terms of reproducibility and robustness, which could pose significant obstacles for their widespread application in academia and industry[26]. In addition, obtaining the accurate Fg value in human is still challenging despite the development of several methods[27].

Therefore, we aimed to establish a reproducible and robust culture method to generate a physiologically relevant in vitro model that can predict drug absorption quantitatively based on FaFg values which can be generally obtained from clinical studies. We adopted a step-by-step approach to select and optimize culture conditions and established a robust and reproducible in vitro model because of the vast number of culture condition combinations that need to be considered[28]. Successfully, we established the reproducible model which can be applied for multiple donors and allows to quantitatively predict drug absorption through a modeling and simulation (M&S) approach.

Results

Development of a robust and reproducible in vitro model for drug absorption

We isolated crypts from the adjacent normal duodenum of surgical specimens and established duodenal organoids (Supplementary Fig. 1a and 1b)[13]. The expression of intestinal stem cell and undifferentiated markers, as well as cell proliferation markers, were higher in these organoids compared to primary enterocytes (Supplementary Fig. 1c). Conversely, the expression of enterocyte markers, drug transporters, and drug-metabolizing enzymes were lower, suggesting that these organoids were predominantly composed of undifferentiated cells. Considering that the organoid cavity corresponds to the digestive tract lumen, we constructed a drug absorption model that can access both luminal (apical) and portal vein (basal) sides using Transwell, a commonly utilized device for drug absorption studies. The specific objective of this experiment was to establish a culture method that demonstrates superior reproducibility and robustness, thus enabling the quantitative prediction of FaFg values. Therefore, the model should possess a tight barrier function, be resistant to artificial bile juice, express absorption-related genes, including *ABCB1* and *CYP3A4*, which encode P-gp and CYP3A4, respectively, exhibit nuclear receptor activity, and provide reproducible and robust results. As a strategic approach to model construction, we defined four key factors that might significantly influence the outcome of cell culture: a) cell digestion to prepare single cells from duodenal organoids, b) extracellular matrix (ECM) coating of Transwell, c) composition of the expansion medium, and d) composition of the differentiation medium. We optimized the culture protocol by verifying the appropriate combination of these factors via four steps and determined the best combination corresponding to the set evaluation points (Fig. 1).

Expansion conditions of human duodenal organoids in the Transwell

In the first step, we focused on the preparation of single cells and the type of ECM (Fig. 1). The cell growth area and transepithelial electrical resistance (TEER) were utilized as evaluation points. TrypLE was used as an enzyme to prepare single cells from organoids, as it increased the cell growth area and TEER value compared with trypsin (Fig. 2a, 2b, Supplementary Fig. 2a, and 2b). Matrigel, collagen I (Col-I), and fibronectin tended to enhance cell expansion and increased TEER values, and iMatrix-511, a recombinant laminin E8 fragment[29], significantly

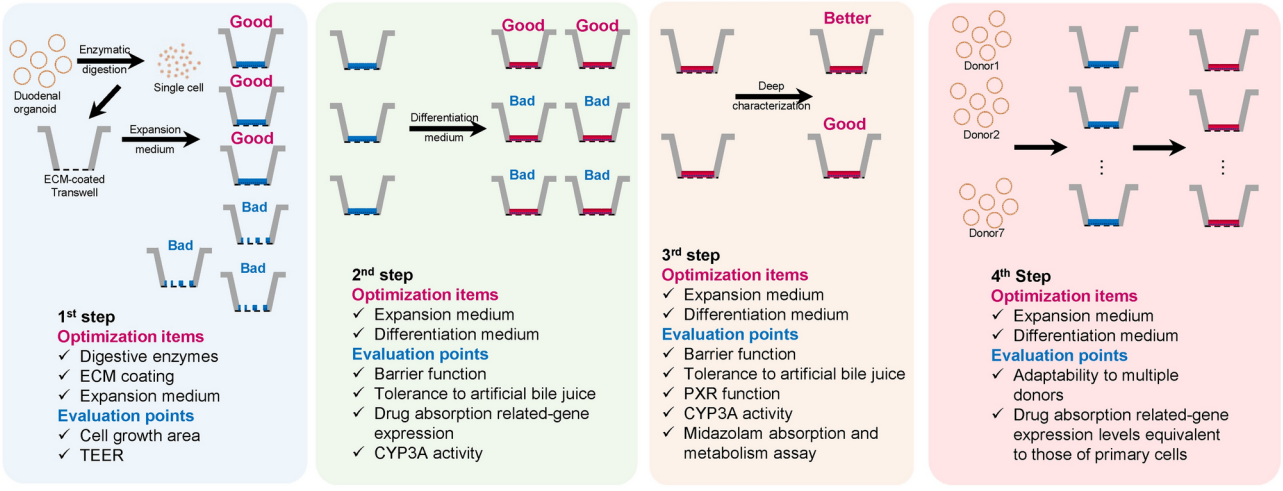

Fig. 1. Overview of establishing the stable monolayer model using human duodenal organoids. ECM, Extracellular matrix; TEER, transepithelial electrical resistance; CYP3A, cytochrome P450 3A; PXR, pregnane X receptor.

increased the cell growth area and TEER value. Considering that duodenal organoids dominantly expressed *ITGA6*, *ITGB1*, and *ITGB4* (Fig. 2c) as well as laminins including laminin-511 that can bind to integrins α6β1 and α6β4[30], we selected Matrigel and iMatrix-511 for ECM coating and TrypLE as the digestive enzyme. Next, we assessed the combined effect of ECM on cell culture outcomes. The combination of iMatrix-511 and fibronectin significantly promoted cell growth (Fig. 2d, 2e, Supplementary Fig. 2c, and 2d). Therefore, we concluded that the combination of iMatrix-511 and fibronectin was an ideal ECM material to expand organoid-derived single cells on the Transwell.

To screen the expansion medium, several media were evaluated (Fig. 2f). The basic composition of the expansion medium was based on what is widely used for intestinal organoid culture[13,17]. We evaluated six types of expansion media (Fig. 2f and Supplementary Fig. 2e). CHIR99021 (CHIR, medium 5), which can enhance Wnt signaling and induce intestinal stem cell proliferation[15], and prostaglandin E2 (PGE2, medium 4), which induces intestinal stem cell differentiation to wound-associated epithelial cells[31], disturbed monolayer formation. Therefore, we selected the top three expansion media—medium 1 (IntestiCult™ + Y), medium 2 (WENRAYg + N_2), and medium 6 (WENRAIFYg)—which increased the TEER value, as candidate expansion media.

Screening of expansion and differentiation media based on multiple evaluation points

As the second step, the differentiation medium was selected based on the three-expansion media (medium 1, 2, and 6). As the evaluation points, we assessed the confirmation of tight barrier function, tolerance to the fasted state simulated intestinal fluid (FaSSIF), expression of drug absorption-related genes, and CYP3A activity (Fig. 1). The maintenance of stemness in the intestinal stem cells is essential for Wnt signaling, and turning off the Wnt signal promotes the differentiation of these cells[13,14]. Furthermore, SB202190 inhibits differentiation into secretory lineage cells, and nicotinamide can enhance long-term maintenance of proliferating intestinal organoids[13,32]. Therefore, we used a medium that excluded Wnt3a, R-spondin1, nicotinamide, and SB202190 as a differentiation medium. Switching to the differentiation medium increased the TEER value; however, medium 2 caused a transient reduction in the TEER value because of cell detachment from the Transwell (Fig. 3a and Supplementary Fig. 3a). The expression of *SI* and *ALPI*, which are enterocyte markers, *ABCB1*, *CYP2C9* and *CYP3A4* were significantly increased compared with those in the organoids owing to differentiation induction (Fig. 3b and Supplementary Fig. 3b). Growth factors such as IGF-1 and FGF2 tended to suppress the increase in the expression of these genes, whereas the N-2 Supplement did not impact gene expression (Fig. 3b and Supplementary Fig. 3b). The total CYP3A activity in each Transwell varied with the type of expansion medium (Fig. 3c and Supplementary Fig. 3c). Considering these results, N-2 Supplement and IGF-1/FGF2 supplementation were considered dispensable, and we selected the ENAg medium as a candidate for the differentiation medium. Medium 2 was excluded because it did not facilitate the formation of stable monolayers. Since Donors 1 and 2 exhibited the same trends, we decided to narrow down the conditions in subsequent assays using only Donor 1.

EGF can affect the differentiation status[33]. Therefore, three types of conditions were examined: Differentiation 1, in which EGF was continuously added; Differentiation 2, in which EGF was removed for 2 days; and Differentiation 3, in which EGF was removed for 3 days. The highest TEER values on day 10 were observed under the combined medium 6 and Differentiation 1 conditions (Fig. 3d). The expression of *SI*, *ABCB1*, *CYP2C19* and *CYP3A4* were higher in the group without EGF, suggesting progressive maturation (Fig. 3e). The CYP3A activity was higher in the group using medium 6 than in the group using medium 1 as the expansion medium (Fig. 3f). We evaluated the barrier function using FaSSIF, and lucifer yellow, a compound that passes through the paracellular route, which represents barrier function. The resistance to FaSSIF was low in the model tested under the Differentiation 3 conditions (Fig. 3g). These results indicate that removing EGF promoted enterocyte maturation, whereas it did not have a substantial impact on CYP3A activity itself and reduced resistance to FaSSIF. In a drug absorption evaluation system, fragile barrier function can negatively impact its reproducibility. Therefore, we finalized medium 6 as the expansion medium and the differentiation medium as either Differentiation 1 or 2.

Detailed analysis of the two culture conditions

In the third step, we comprehensively evaluated the activity of pregnane X receptor (PXR), an important nuclear receptor in drug–drug interactions, and midazolam, a typical CYP3A substrate drug, under the two culture conditions using FaSSIF buffer (Fig. 1). PXR induces the expression of drug transporters and metabolizing enzymes when treated with representative substrates such as rifampicin and causes drug–drug interaction effects such as reduction in the blood concentration of co-administered drugs in clinical settings. Rifampicin induced drug transporters and metabolizing enzymes and significantly increased CYP3A activity under both Differentiation 1 and 2 culture conditions (Fig. 4a and 4b). It dramatically increased the expression of the drug transporter *ABCC2* and *CYP3A4*. Furthermore, in the midazolam absorption assay, rifampicin exposure reduced midazolam absorption and increased the production of its metabolite, 1′-hydroxymidazolam (1′-OH midazolam), under both Differentiation 1 and 2 conditions (Fig. 4c and 4d). 1′-OH midazolam was detected on both sides of the Transwell, implying that not all 1′-OH midazolam produced via metabolism were absorbed into the portal vein; some were excreted into the intestinal lumen (Fig. 4d). The TEER value increased with increasing numbers of differentiation days regardless of rifampicin addition, whereas the TEER value varied on day 10 under Differentiation 2 conditions (Fig. 4e). A similar trend was observed in resistance to FaSSIF (Fig. 4f). Under other conditions, the robust barrier function was stably maintained (Fig. 4e and 4f). These results suggested both monolayer cultures expressed a functional PXR; however, from the perspective of maintaining stable barrier function, the Differentiation 1 condition may be superior. Consequently, we established the Differentiation 1 condition as the standard for differentiation.

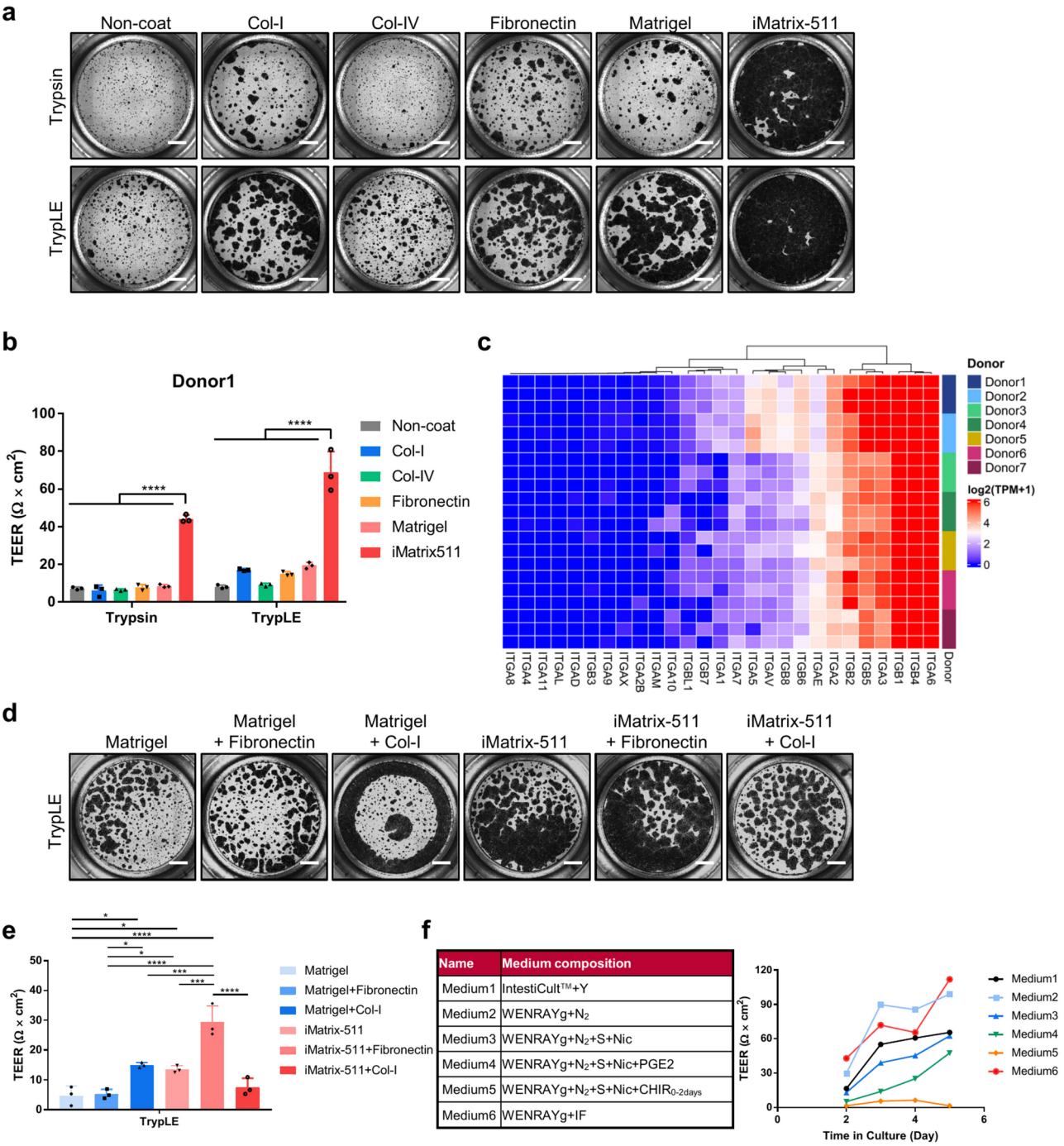

Name	Medium composition
Medium1	IntestiCult™+Y
Medium2	WENRAYg+N_2
Medium3	WENRAYg+N_2+S+Nic
Medium4	WENRAYg+N_2+S+Nic+PGE2
Medium5	WENRAYg+N_2+S+Nic+$CHIR_{0\text{-}2days}$
Medium6	WENRAYg+IF

Adaptability to multiple donors and further improvements

Intestinal organoids have varying proliferative properties depending on the strain (Supplementary Fig. 4a). Therefore, as the fourth step, we used organoids derived from seven donors to verify whether the selected culture condition (TrypLE × iMatrix-511/fibronectin × Medium 6 × Differentiation 1) could be applied to seven organoids. A confluent monolayer was formed in donor 1 and 6 organoids during the 4-day expansion period, whereas the others did not form a confluent monolayer (Fig. 5a). Therefore, further improvements were necessary; the addition of AlbuMAX, a lipid-rich albumin, dramatically improved the efficiency of monolayer formation (Fig. 5a). The addition of AlbuMAX increased the proliferative cell count (Fig. 5b). Additionally, AlbuMAX increased the TEER values in a concentration-dependent manner and improved resistance to FaSSIF (Fig. 5c, 5d, and Supplementary Fig. 4b). The lucifer yellow permeability among multiple donors were low in the presence of AlbuMAX and were similar, which indicated that a confluent monolayer could eventually be formed under any donor condition by switching to a differentiation medium (Fig. 5d). Furthermore, it significantly increased the expression of the *ABCG2*, *CES2*, *CYP2D6*, *CYP3A4*, *UGT1A1*, *UGT1A10*, and *UGT2B7*, strongly suggesting its usefulness (Fig. 5e). To identify the active ingredients in AlbuMAX, we verified whether bovine serum albumin (BSA) and the various lipid components have similar effects. Monolayer formation did not improve under culture conditions combining BSA, free fatty acid (FFA), phospholipid, and cholesterol (Cho)

◀**Fig. 2**. Assessment of expansion conditions of human duodenal organoid-derived cells as the first step. (**a**) Bright-field images of monolayer culture derived from donor 1 when the Transwell was coated with different ECMs. Monolayer cultures were subjected to MTT staining assay on day 8. Scale bars, 1 mm. Col-I; Collagen I, Col-IV; collagen IV. (**b**) TEER values of the monolayer cultures on day 8 (n = 3). The commercially available medium IntestiCult™ (STEMCELL Technologies) supplemented with a ROCK inhibitor Y-27632 to prevent anoikis was used to seed single cells in the Transwell and as an expansion medium. (**c**) Heatmap depicting the expression of integrin in duodenal organoids derived from multiple donors based on the RNA sequencing results (n = 3). Heat map was created using ComplexHeatmap package version 2.14.0 (https://www.bioconductor.org/packages/release/bioc/html/ComplexHeatmap.html). Red shows high expression, whereas blue shows low expression. (**d**) The bright-field images of the monolayer culture derived from donor 1 when the Transwell was coated with different ECMs. Monolayer cultures were subjected to MTT staining assay on day 4. Scale bars, 1 mm. (**e**) TEER values of the monolayer cultures on day 4 (n = 3). (**f**) The table of the medium composition for each culture condition from Medium 1 to Medium 6 and the measurements of TEER values (n = 2). W, Afamin/Wnt3a CM; E, EGF; N, Noggin; R, R-spondin-1; A, A83-01; Y, Y-27632; g, Gastrin I; N_2, N-2 supplement; S, SB202190; N, nicotinamide; PGE2, prostaglandin E2; CHIR, CHIR99021; I, IGF-1; F, FGF2. $CHIR_{0\text{-}2\ days}$ indicates supplementation with CHIR for the first 2 days of culture. The *P* value was determined by one-way ANOVA with Tukey's multiple comparison test.

(Supplementary Fig. 4c and 4d). Similar trends were observed with PPARδ (GW501516) and GPR40 agonists (TAK-875), which are receptors for FFAs (Supplementary Fig. 4c)[34]. However, when the donor 1 sample, which formed a monolayer even without AlbuMAX, was used, the TEER value increased with the addition of FFAs, except for palmitic acid, during the differentiation period (Supplementary Fig. 4e). These effects were also observed with GW501516 and TAK-875 (Supplementary Fig. 4f. and 4 g). These results suggested dual effects of AlbuMAX: accelerated monolayer formation and increased TEER value. The increase in TEER value could be attributed to effects of the FFA present in AlbuMAX, and the promotion of monolayer formation could be attributed to components other than BSA, FFA, phospholipid, and Cho.

A comparison of the expression of the key genes involved in drug absorption between the established model and primary enterocytes showed lower expression of several genes (Fig. 5h). 1α, 25-dihydroxyvitamin D3 (VD3) is an endogenous compound and is known to enhance *ABCC2*, *CYP2C*, and *CYP3A4* expression via the nuclear receptor vitamin D receptor (VDR)[1,35,36]. Addition of VD3 increased the expression of several genes and CYP3A activity in a concentration-dependent manner (Fig. 5f and 5g). At 100 nM, the expression of the absorption-related genes, including *ABCC2* and *CYP3A4*, which were low in the absence of VD3, increased to levels comparable to those in primary enterocytes (Fig. 5h). These results indicated that our model possessed a functional VDR, and that VD3 addition elicited the expression and activity of key factors involved in drug absorption. Therefore, we added 100 nM VD3 to our finalized culture conditions.

Characteristics of the human intestinal organoid-derived monolayer model

We next characterized our model in several aspects. The tight junction marker, zonula occludens-1 (ZO-1), and the adherence junction marker, E-cadherin, were expressed between cells (Fig. 6a), and a distinct tight junction structure was confirmed through transmission electron microscopy (Fig. 6d). Additionally, MUC2-positive goblet cells, and cells with a short microvilli and secretory granule-like structure, were identified (Fig. 6b and 6e). The cells exhibited a columnar shape, with nuclei localized on the basal side, polarized localization of ZO-1, and F-actin-positive microvilli structures on the luminal side of the monolayer (Fig. 6c and 6d). These results indicated that the morphology of the model was strikingly similar to that of in vivo intestinal epithelial cells.

P-gp and BCRP function was assessed via efflux assays with or without inhibitors. P-gp substrate digoxin transport was canceled by inhibitor zosquidar (Fig. 6f). BCRP substrate sulfasalazine transport was blocked by inhibitor Ko143 (Fig. 6g). These results indicated functional P-gp and BCRP in the monolayer model. Next, we verified uridine diphosphate glucuronosyl-transferase (UGT) function using raloxifene. Raloxifene is metabolized by UGT, resulting in the formation of 6-gluculonide and 4′-glucuronide. Raloxifene was mostly found to be metabolized to glucuronide (Fig. 6h). Irinotecan is metabolized by carboxylesterase2 (CES2) to form the active metabolite SN-38; thus, CES2 is an important hydroxylase when considering such a prodrug approach. In our model, the metabolite SN-38 was detectable, and its generation was significantly inhibited by loperamide, a CES2 inhibitor (Fig. 6i). Next, we performed a permeability assay using midazolam and 1-aminobenzotriazole (ABT), a pan-CYP inhibitor. Midazolam metabolites were detected, and the amount of 1′-OH midazolam was comparable to that of midazolam (Fig. 6j). In the presence of ABT, the amount of metabolites significantly decreased with a corresponding increase in the amount of midazolam (Fig. 6j). Consistent with these results, midazolam permeability was significantly enhanced by ABT (Fig. 6k). The amount of midazolam that disappeared from the apical side was similar to the total amount of midazolam that permeated to the basal side and the metabolites detected on both basal and apical sides (Supplementary Fig. 5).

Finally, we evaluated the PXR function. The induction effect of rifampicin was confirmed upon VD3 addition, and the gene expression levels significantly increased (Fig. 6l). These results indicated that our model possessed the characteristics of various absorption-related key factors that play important roles in intestinal absorption.

Robustness and reproducibility of the novel absorption model

The robustness and reproducibility of the in vitro model are key factors for practical application in drug discovery research. We evaluated the intra- and inter-experiment variations (Fig. 7 and Supplementary Fig. 6). Barrier function reproducibility is the most crucial factor in an absorption evaluation assay. Our model demonstrated

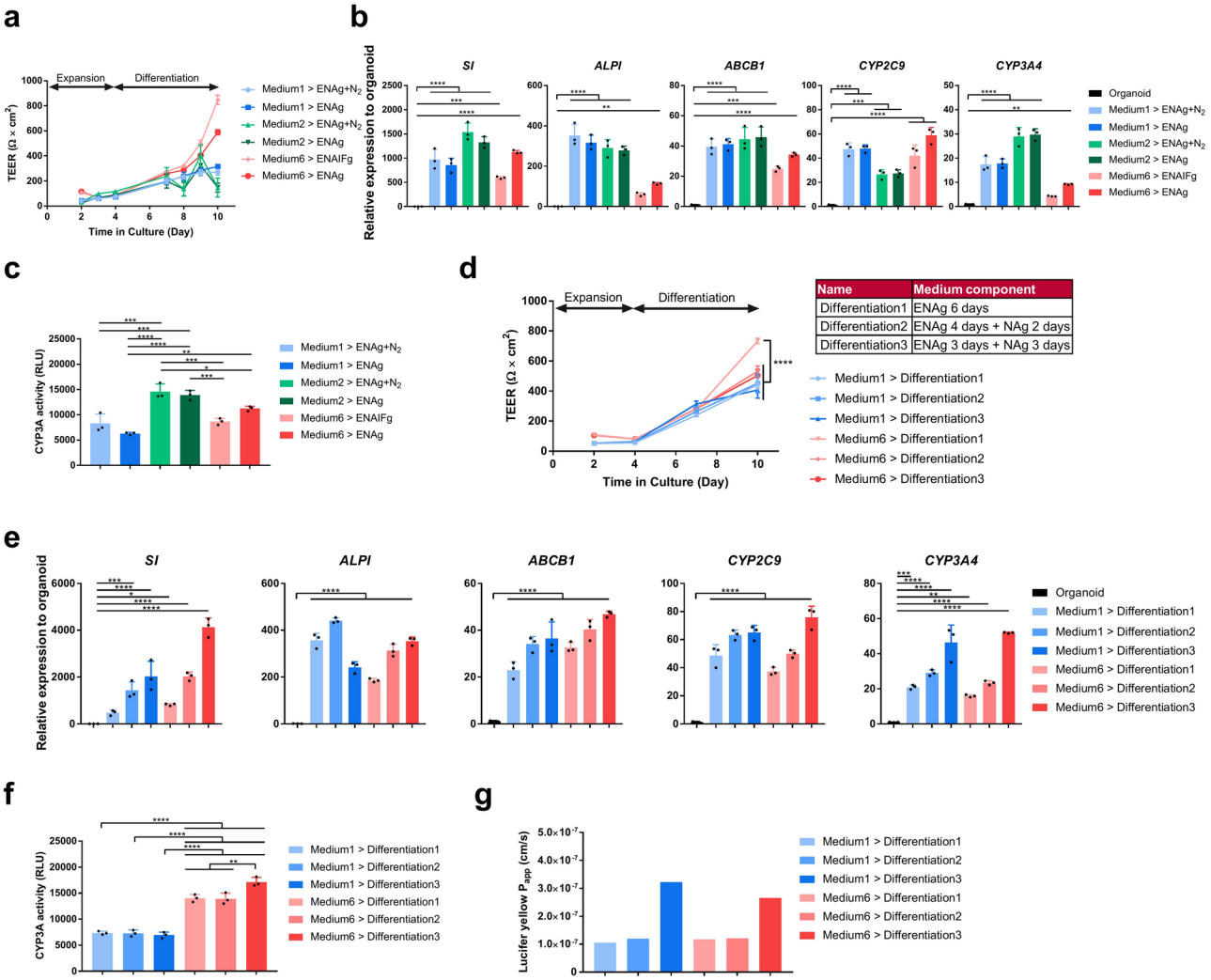

Fig. 3. Determination of expansion and differentiation media combination in the second step. (**a**) TEER values during the expansion and differentiation processes (n = 3). (**b**) Relative gene expression in each expansion and differentiation condition in monolayer cultures derived from donor 1 determined by quantitative RT-PCR (n = 3). The *P* value was determined by one-way ANOVA with Dunnett's multiple comparison test. (**c**) CYP3A activity in monolayer cultures as determined by P450-Glo™ CYP3A4 Luciferin-IPA assay (n = 3). The *P* value was determined by one-way ANOVA with Tukey's multiple comparison test. (**d**) Compositions of the differentiation medium for each culture condition from Differentiation 1 to Differentiation 3 and the measurements of TEER values during the expansion and differentiation processes (n = 3). The *P* value was determined by one-way ANOVA with Tukey's multiple comparison test. (**e**) Relative gene expression as determined by quantitative RT-PCR (n = 3) in each expansion and differentiation condition in monolayer cultures derived from donor 1. The *P* value was determined by one-way ANOVA with Dunnett's multiple comparison test. (**f**) CYP3A activity in monolayer cultures determined by P450-Glo™ CYP3A4 Luciferin-IPA assay (n = 3). The *P* value was determined by one-way ANOVA with Tukey's multiple comparison test. (**g**) The P_{app} value of lucifer yellow in artificial bile acid (FaSSIF) resistance assay (n = 1). E, EGF; N, Noggin; A, A83-01; N_2, N-2 supplement; g, Gastrin I; I, IGF-1; F, FGF-2.

a robust and uniform barrier function in intra-experiment comparisons, showing a low coefficient of variation (CV) value of 8.6% (Fig. 7a). Generally, the criterion of the lucifer yellow P_{app} value in permeability assay using Caco-2 model is set to below 1.0×10^{-6} cm/s. The lucifer yellow P_{app} value met these criteria within individual experiments as well as inter-experiments (Fig. 7b). We then evaluated the reproducibility of the effects of VD3. The effect was consistently observed in the inter-experiment comparisons for the two donors (Fig. 7c). Next, we evaluated the intra- and inter-experimental variations in the absolute gene expression values. Almost all intra-experimental gene expression levels varied within ± 1.5-fold (Fig. 7d). Moreover, the reproducibility of our results was also commendable between experiments and among donors since the average intra-experimental and inter-experimental values varied within ± 1.5 times (Supplementary Fig. 6). Finally, we assessed the reproducibility of CYP3A function in donor 1 using midazolam, focusing on permeability and metabolite production. The P_{app} value of midazolam and the production of 1′-OH midazolam were within the mean ± 1.5-fold change within

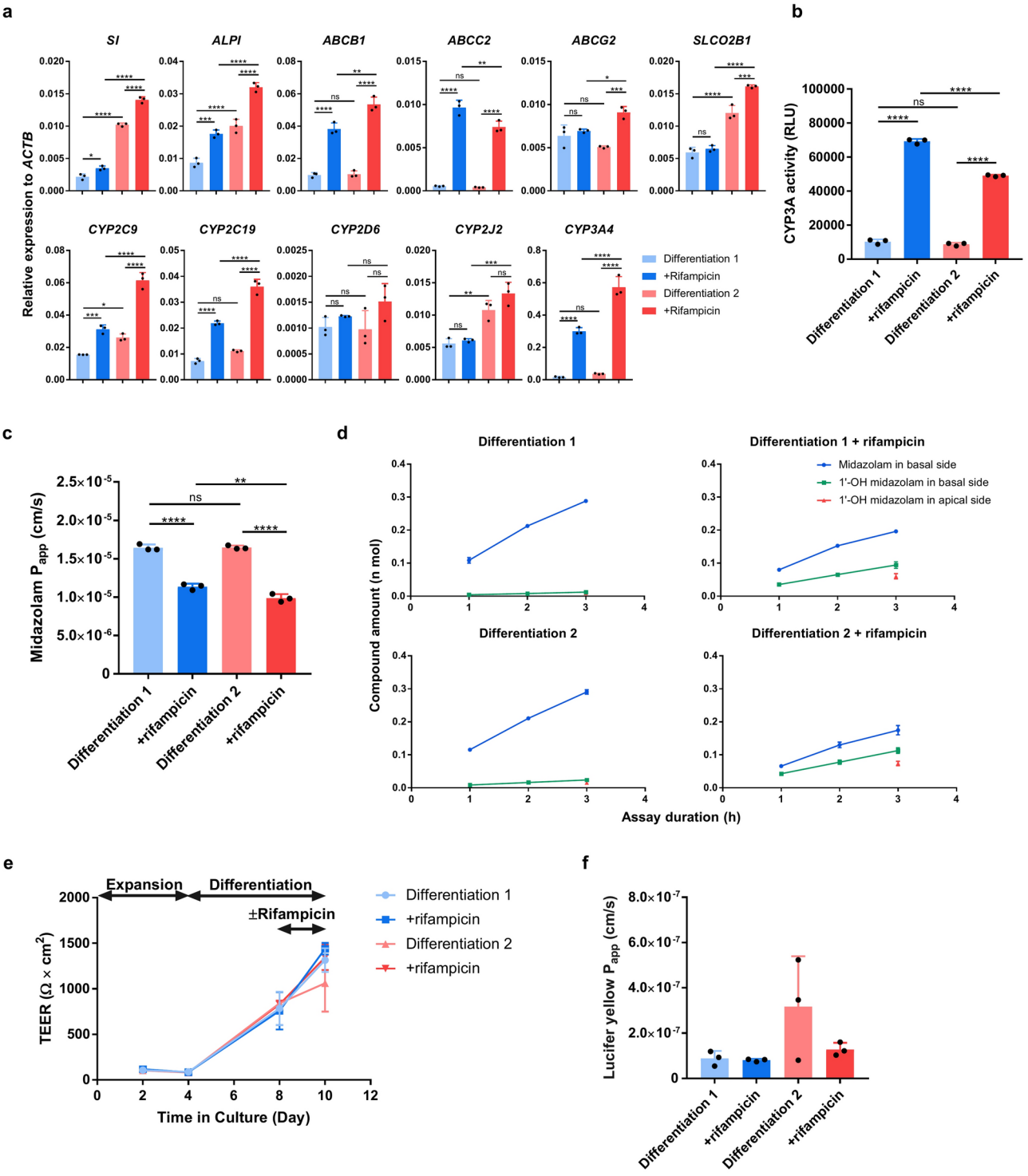

Fig. 4. In-depth characterization and comparative analysis of two culture conditions in the third step. (**a**) Gene expression relative to *ACTB* expression obtained by quantitative RT-PCR in the presence or absence of rifampicin (n = 3). Cells were exposed to 10 µM rifampicin during the last two days of the differentiation process. (**b**) CYP3A activity in monolayer cultures determined by P450-Glo™ CYP3A4 Luciferin-IPA assay (n = 3). (**c**) The P_{app} value of midazolam with or without rifampicin induction (n = 3). (**d**) Time-dependent translocation of midazolam from the apical compartment to the basal compartment and the amount of 1′-hydroxymidazolam (1′-OH midazolam) generated in both apical and basal compartments (n = 3). (**e**) TEER values during the expansion and differentiation processes with or without rifampicin induction (n = 3). (**f**) The P_{app} value of lucifer yellow with or without rifampicin induction in artificial bile acid (FaSSIF) resistance assay (n = 3). The *P* value was determined by one-way ANOVA with Tukey's multiple comparison test.

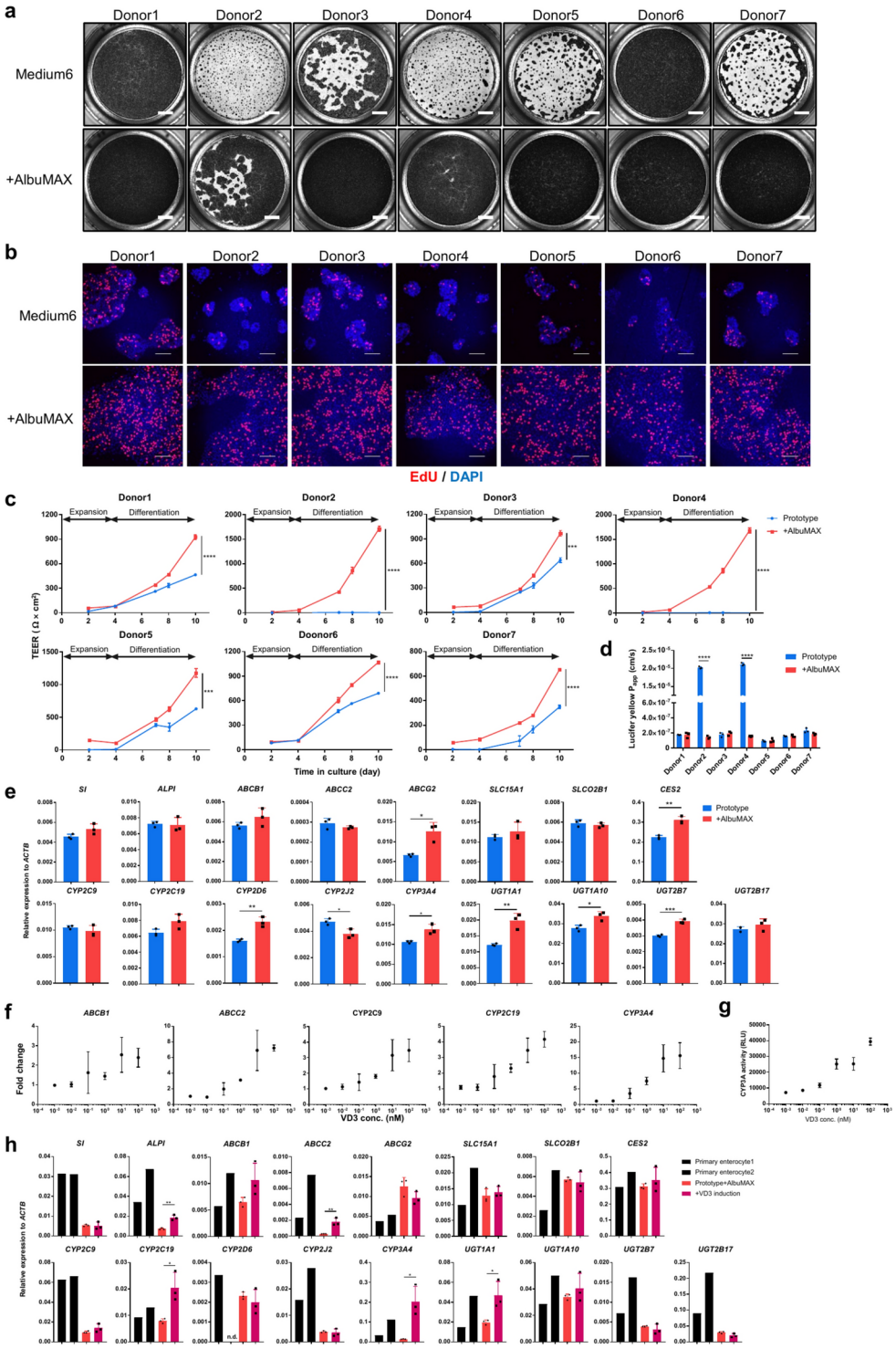

Fig. 5. Additional optimization of medium components in the fourth step. (**a**) The bright-field images of monolayer culture derived from donors 1 to 7 using medium 6 with or without 4 mg/mL AlbuMAX in the expansion phase. Monolayer cultures were subjected to MTT staining assay on day 4. Scale bars, 1 mm. (**b**) Fluorescent images of the EdU uptake by monolayer culture derived from donors 1 to 7. Scale bars, 100 µm. (**c**) TEER values during the expansion and differentiation processes (n = 3). (**d**) The P_{app} value of lucifer yellow in artificial bile acid (FaSSIF) resistance assay (n = 3). (**e**) Gene expression level relative to *ACTB* expression as determined by quantitative RT-PCR (n = 3). (**f**) Relative gene expression after adding various concentrations of 1α, 25-dihydroxyvitamin D3 (VD3) (n = 3). VD3 was added during the last two days of the differentiation process. (**g**) CYP3A activity of monolayer cultures determined by P450-Glo™ CYP3A4 Luciferin-IPA assay (n = 3). (**h**) Relative gene expression of the organoid-derived model and primary enterocytes. The *P* value was determined by a two-tailed unpaired *t*-test.

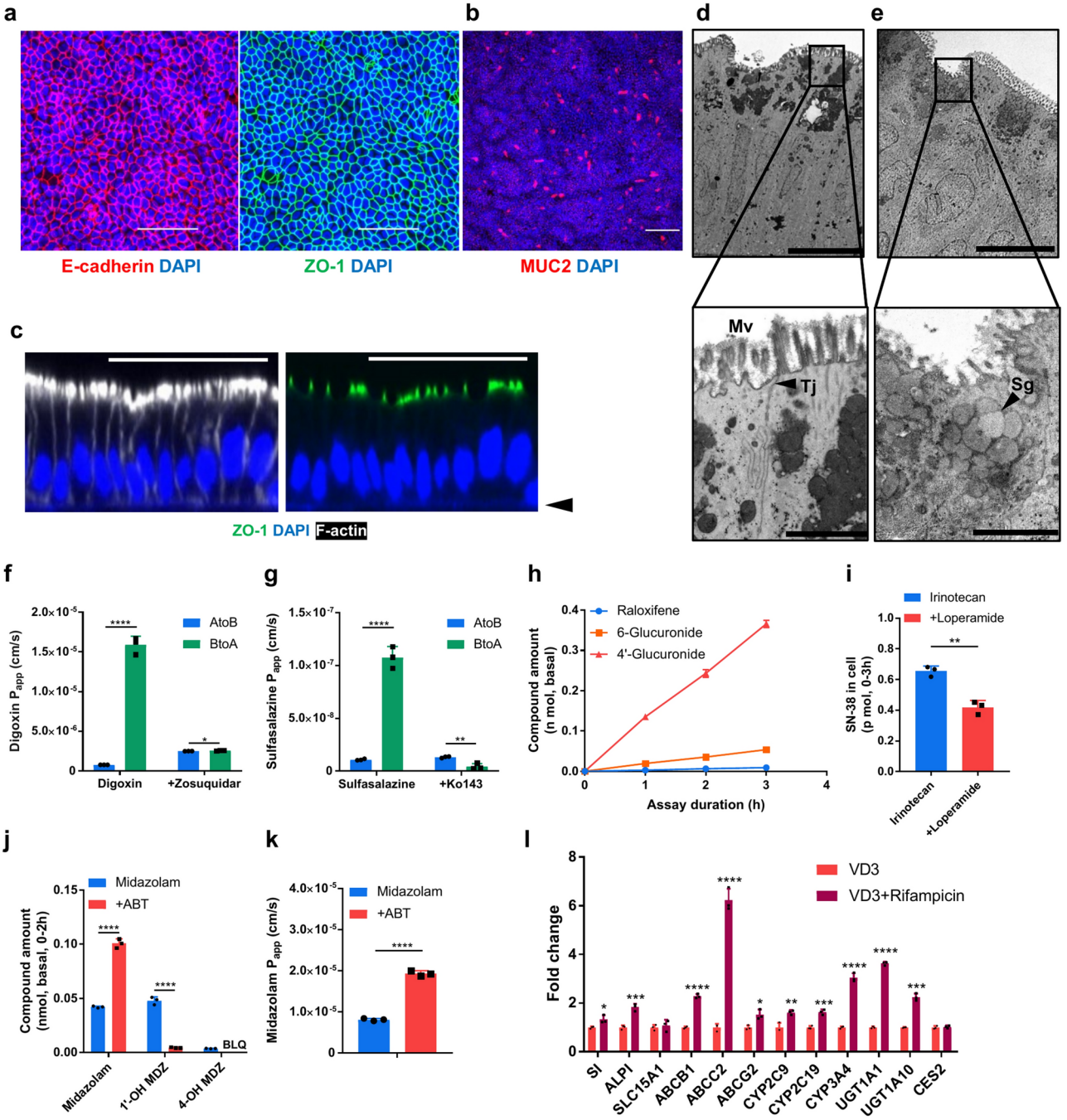

Fig. 6. Characterization of the novel human duodenal organoid-derived monolayer model. (**a**) Immunofluorescence analysis for E-cadherin (red), ZO-1 (green), (**b**) MUC2 (red), and nucleus (blue). Scale bars, 100 µm. (**c**) Immunofluorescence analysis depicting cross sections of the monolayer model; ZO-1 (green), nucleus (blue), and F-actin (white). Scale bars, 100 µm. Black arrows indicate the Transwell membrane. (**d**) and (**e**) Transmission electron microscopic analysis of the monolayer model. Mv, microvilli; Tj, tight junction; Sg, secretory granule-like structures. Scale bars, 10 µm for low magnification images and 2 µm for high magnification images. (**f**) Efflux transporter P-gp assay using the P-gp substrate digoxin with or without zosuquidar as an inhibitor. AtoB, apical to basal; BtoA, basal to apical. (**g**) Efflux transporter assay using BCRP substrate sulfasalazine with or without Ko143. (**h**) UDP-glucuronosyltransferase (UGT) functional assay using raloxifene as a UGT substrate. (**i**) Carboxylesterase 2 (CES2) functional assay using irinotecan as a substrate with or without loperamide as an inhibitor. The amount of SN-38, a metabolite of irinotecan, was detected in the cells of the monolayer model. (**j**) and (**k**) Midazolam permeability and metabolism assay using 2 µM midazolam as a substrate of CYP3A with or without 1-aminobenzotriazole (ABT) as a pan-CYP inhibitor. BLQ, below limit of quantification. (**l**) Relative gene expression determined by quantitative RT-PCR of the monolayer model with induction of VD3 or VD3 + rifampicin. Cells were treated with inducers for the last two days of the differentiation process. The *P* value was determined by a two-tailed unpaired *t*-test.

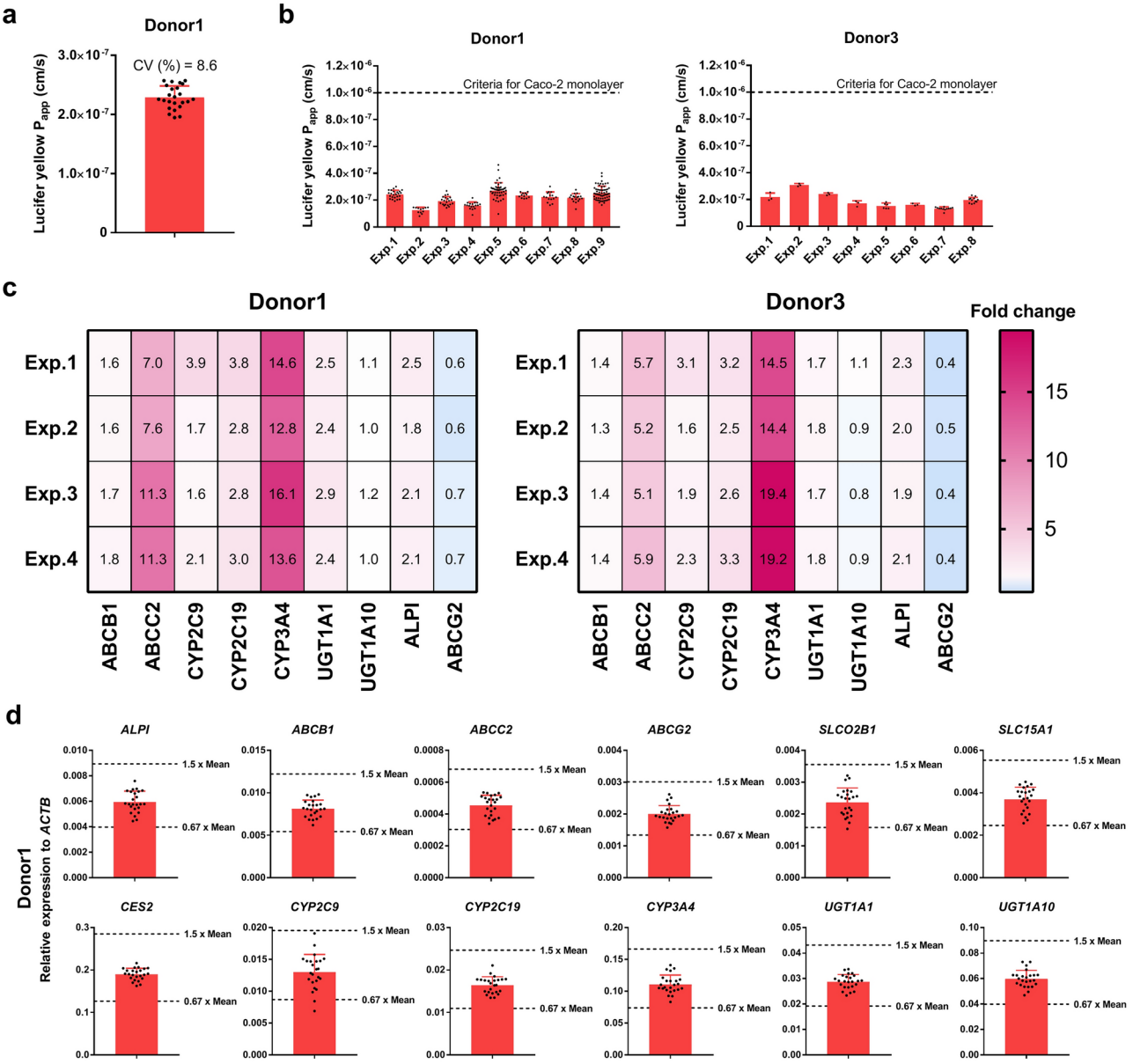

Fig. 7. Assessment of the reproducibility and robustness of the novel monolayer model. (**a**) The FaSSIF tolerability assay using lucifer yellow as a barrier integrity marker in an intra-individual experiment on donor 1 (n = 24). (**b**) FaSSIF tolerability assay in inter-individual experiments of donor 1 and donor 3 (donor1: exp.1, n = 16; exp.2, n = 12; exp.3, n = 21; exp.4, n = 18; exp.5, n = 48; exp.6, n = 12; exp.7, n = 15; exp.8, n = 18; exp.9, n = 60, donor2: exp.1, n = 2; exp.2–6, n = 3; exp.7 and exp.8, n = 12). Exp.; experiment. (**c**) Heat map of the relative expression of each gene following VD3 induction, compared to non-induction conditions of donor 1 and donor 3 in inter-individual experiments. The values represent the mean of biological replicates in each experiment (n = 3). Heat map was created using GraphPad Prism 7.04 (https://www.graphpad.com/) (**d**) Relative gene expression profiles determined by quantitative RT-PCR of the monolayer model in intra-individual experiments following VD3 induction (n = 24). The dotted lines represent ± 1.5-fold of the mean values.

inter-experiments (Supplementary Fig. 7). These results suggested that our culture method could generate the monolayer culture with high reproducibility.

Donor-to-donor variation in drug absorption profiles

To investigate inter-organoid variation in drug absorption, we evaluated the absorption of 19 commercially available drugs using a four-donor-derived monolayer model. No notable differences in P_{app} were observed between the drugs that showed high P_{app} values (ketoprofen, rosiglitazone, carbamazepine, antipyrine, theophylline, pitavastatin, glimepiride, metoprolol, propranolol; $P_{app} > 1.0 \times 10^{-6}$ cm/s), and these drugs exhibited good absorption properties (Supplementary Fig. 8a). In contrast, significant differences were observed among

the drugs that showed relatively low P_{app} values ($P_{app} < 1.0 \times 10^{-6}$ cm/s) except oxacillin (Supplementary Fig. 8a). Drug absorption is affected by drug transporters and metabolizing enzymes. We observed several differences of gene expression among donors (Supplementary Fig. 8b). Notably, none of the donors exhibited uniformly high expression of all genes, indicating that expression patterns varied depending on the genes. We conducted additional evaluations to determine whether inter-organoid variability existed in the functions of P-gp, BCRP, and CYP3A in these differentially expressed genes. As expected, absorption of the P-gp substrate digoxin differed among donors, absorption increased with the addition of P-gp inhibitors, and the expression of *ABCB1* and genes involved in digoxin absorption were negatively correlated (Supplementary Fig. 8c). Similarly, the absorption of sulfasalazine differed among donors, and these differences disappeared in the presence of BCRP inhibitors; a negative correlation was also observed (Supplementary Fig. 8d). The absorption of midazolam, differed among the four donors, and the addition of pan-CYP inhibitors eliminated these differences. The production of the metabolite of differed significantly among the four donors, and the addition of an inhibitor significantly inhibited this production (Supplementary Fig. 8e and 8f.). These results indicated that the monolayers derived from four donors exhibited different drug absorption properties.

Estimation of human drug absorption rate

We next verified whether the permeability of commercially available drugs through the monolayer model reflected their in vivo absorption in humans. Initially, we developed an in vitro permeability test and described human in vivo absorption using mathematical models (Fig. 8a and 8b). By combining the parameters of these two models under several assumptions, we developed a theory to estimate the drug absorption rate from its permeability. To validate this theory, we evaluated the permeability of launched 19 drugs with reported human Fa values[37]. A positive correlation was observed between their permeability and Fa (Fig. 8c and 8e). Furthermore, by optimizing the parameter Q/S in Eq. (22) described in the Methods section to 3.04×10^{-7} cm/s, a regression curve with a good correlation coefficient was obtained (Fig. 8e). Digoxin, a typical P-gp substrate exhibited values that were in alignment with the regression curve (Fig. 8e), there was no substantial deviation between the estimated FaFg value and the in vivo FaFg value (Fig. 8d–f, Method 1). In contrast, when we verified the correlation between the in vitro permeability and in vivo FaFg for six typical CYP3A substrates and two P-gp & CYP3A substrate, the result deviated from the permeability-Fa regression curve of the aforementioned 19 drugs, and the FaFg of the six CYP3A substrates and tacrolimus (P-gp & CYP3A substrate) estimated from this curve tended to be overestimated (Fig. 8d–f, Method 1). Thereafter, we investigated the ability of another estimation method described as Eq. (21), using the permeability data for the six CYP3A substrates, one P-gp substrate, and two P-gp & CYP3A substrates with or without the pan-CYP inhibitor ABT. Only three drugs had an estimation accuracy of 1.5 times, and the FaFg was underestimated for six out of nine drugs (Fig. 8d and 8f, Method 2). To consider the difference in the CYP3A activity between the monolayer model and in vivo enterocytes, we defined the average CYP3A4 expression in primary enterocyte1 and primary enterocyte2 as the expression in in vivo enterocytes (Fig. 5h). Upon comparison with CYP3A4 expression in the monolayer model derived from donor 1, it was observed that CYP3A4 expression in in vivo enterocytes was 0.24 times that of the monolayer model. Assuming this expression ratio to be equivalent to the ratio between the in vitro and in vivo activity and incorporating it into Eq. (20), we estimated the value of FaFg. The estimated FaFg for seven of nine drugs fell within an estimated accuracy of 1.5 times compared with the observed values including the CYP3A substrates, P-gp substrate, and P-gp & CYP3A substrates (Fig. 8d and 8f, Method 3), suggesting that our in vitro model-based experimental system can accurately predict the drug absorption.

Discussion

The drug development process necessitates a comparative analysis of hundreds to thousands of candidate drugs to select those possessing superior profiles. In this context, the reproducibility and robustness of in vitro models have emerged as pivotal components for appropriate evaluation. In this study, we successfully constructed a reproducible and robust absorption model, which exhibited characteristics emulating human intestine. Using a step-by-step approach based on the fit-for-purpose, we efficiently optimized the culture conditions. We believe that it is crucial to adopt such a strategy to develop advanced in vitro culture systems with high reproducibility.

In the first step, we found that TrypLE, and a combination of iMatrix-511 and fibronectin, demonstrated superior efficiency in promoting monolayer formation. Laminin and fibronectin are important ECM components in human intestine, and duodenal organoids express the integrin a5b1, which can bind fibronectin[38,39]. In the second step, we selected two cultivation conditions by evaluating the characteristics of the model from various perspectives. The evaluation of the combination of expansion and differentiation media suggested that determining the expansion medium based only on the results in the expansion phase might lead to misleading conclusions. In the third step, we further narrowed down the appropriate conditions for the absorption evaluation model. The results suggest that the withdrawal of growth factors promoted cell differentiation and reduced FaSSIF resistance. We eventually selected Differentiation 1 condition because establishing conditions that can balance the barrier function and gene expression as well as function of absorption-related molecules, including CYP, was crucial in setting reproducible and robust culture conditions for a drug absorption assay. This trend was also observed in our previous study[40]. In the fourth step, we found that AlbuMAX was a critical component in adapting the culture method to cells prepared from organoids derived from various donors. Our findings indicated that specific unsaturated fatty acids increased the TEER value; however, we were unable to identify the components that promote proliferation in the expansion phase. Several reports have demonstrated that AlbuMAX promotes cell differentiation and self-renewal of stem cells[41–43]. AlbuMAX contains several lipids such as lysophosphatidic acid and sphingosine-1-phosphate (S1P), which are signaling lipids that regulate various physiological process[42]. These signaling molecules might be key factors in AlbuMAX. Further investigation to

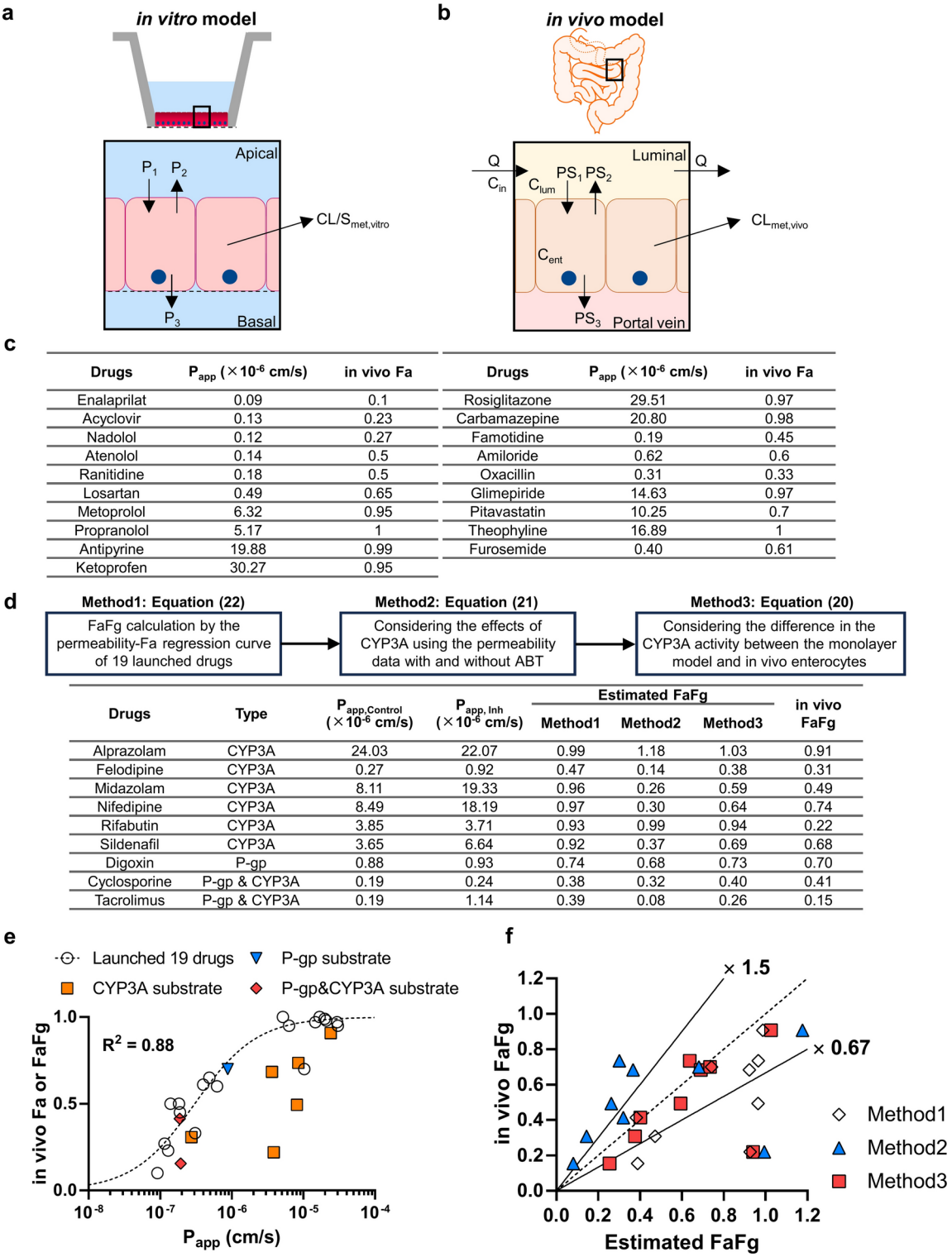

c

Drugs	P_{app} (×10^{-6} cm/s)	in vivo Fa	Drugs	P_{app} (×10^{-6} cm/s)	in vivo Fa
Enalaprilat	0.09	0.1	Rosiglitazone	29.51	0.97
Acyclovir	0.13	0.23	Carbamazepine	20.80	0.98
Nadolol	0.12	0.27	Famotidine	0.19	0.45
Atenolol	0.14	0.5	Amiloride	0.62	0.6
Ranitidine	0.18	0.5	Oxacillin	0.31	0.33
Losartan	0.49	0.65	Glimepiride	14.63	0.97
Metoprolol	6.32	0.95	Pitavastatin	10.25	0.7
Propranolol	5.17	1	Theophyline	16.89	1
Antipyrine	19.88	0.99	Furosemide	0.40	0.61
Ketoprofen	30.27	0.95			

d

Method1: Equation (22): FaFg calculation by the permeability-Fa regression curve of 19 launched drugs

Method2: Equation (21): Considering the effects of CYP3A using the permeability data with and without ABT

Method3: Equation (20): Considering the difference in the CYP3A activity between the monolayer model and in vivo enterocytes

Drugs	Type	$P_{app,Control}$ (×10^{-6} cm/s)	$P_{app,Inh}$ (×10^{-6} cm/s)	Estimated FaFg			in vivo FaFg
				Method1	Method2	Method3	
Alprazolam	CYP3A	24.03	22.07	0.99	1.18	1.03	0.91
Felodipine	CYP3A	0.27	0.92	0.47	0.14	0.38	0.31
Midazolam	CYP3A	8.11	19.33	0.96	0.26	0.59	0.49
Nifedipine	CYP3A	8.49	18.19	0.97	0.30	0.64	0.74
Rifabutin	CYP3A	3.85	3.71	0.93	0.99	0.94	0.22
Sildenafil	CYP3A	3.65	6.64	0.92	0.37	0.69	0.68
Digoxin	P-gp	0.88	0.93	0.74	0.68	0.73	0.70
Cyclosporine	P-gp & CYP3A	0.19	0.24	0.38	0.32	0.40	0.41
Tacrolimus	P-gp & CYP3A	0.19	1.14	0.39	0.08	0.26	0.15

Fig. 8. Prediction of human drug absorption by combining modeling & simulation and the organoid-derived model. (**a**) Mathematical modeling of the in vitro and (**b**) in vivo absorption of drugs. The detailed equations are described in the Methods. (**c**) The geomean of P_{app} values of the 19 launched drugs in the donor 1-derived monolayer model and the in vivo Fa value[37]. (**d**) The flow diagram of calculation methods of Method 1 to Method 3 and the geomean of P_{app} values of six typical CYP3A4 substrates, one typical P-gp substrate, and two P-gp & CYP3A dual substrates with or without ABT as an inhibitor, estimated FaFg values calculated using Methods 1 to 3, and in vivo FaFg values[58]. $P_{app, Control}$, P_{app} values without inhibitor; $P_{app, Inh}$, P_{app} values with inhibitor (ABT). (**e**) The correlation plot of the in vivo Fa or FaFg values and P_{app} values. (**f**) The correlation plot of the in vivo FaFg values and in vitro estimated FaFg values calculated by each method. The solid line indicates unity, and dotted lines represent a range of ± 1.5 times.

elucidate the active lipids could pave the way for substantial advancements in the refinement of culture medium components.

Drug absorption in humans is subject to considerable inter-individual variation. In this study, we observed differences in the expression profiles of absorption-related key genes among organoids, as well as different drug absorption properties. Drug absorption varies both between individuals and within individuals and is markedly influenced by various factors, including composition and volume of intestinal fluid, pH, osmolality, diet, and microbiome[44]. Thus, it is unlikely that the organoid models can perfectly mimic drug absorption in patients. Intestinal organoids can maintain their genetic and epigenetic profiles[18,45]. Inter-individual differences in single nucleotide polymorphisms (SNPs) and epigenetic status can substantially affect drug absorption[46–48]. Various donor-derived organoids can be utilized to elucidate these differences.

To estimate the Fa and FaFg of drugs in vivo in humans using their permeability determined based on the monolayer model, we conducted a theoretical study using mathematical models. Previous studies have theoretically estimated the Fg of CYP3A substrates[24]. We extended this to FaFg estimation in this study. Generally, obtaining reliable in vivo Fg values is challenging because it requires referencing information from pharmacokinetic studies following intravenous and oral administration, as well as from clinical pharmacological studies conducted under special conditions. In contrast, the FaFg is more suitable for verifying our estimation theory because it can be calculated by dividing the bioavailability by hepatic availability, making it relatively easy to obtain a reliable value. An earlier verification with 19 drugs indicated that the permeability in the monolayer model showed good correlation to their Fa in humans in vivo. We constructed a regression curve of the permeability and Fa with a high correlation coefficient using the relationship derived from the mathematical model and the optimized coefficients, which suggested that these relationships were theoretically valid. The R^2 value of 0.88 is comparable to or superior to the R^2 value calculated using almost the same launched drugs in the Caco-2 model previously[37], demonstrating that it possesses predictive accuracy for Fa values that is at least equivalent to that of the Caco-2 model. The estimated FaFg value for digoxin, a typical substrate of P-gp, calculated using this regression curve, demonstrated a value comparable to that observed in humans. This result indicates that this model can be extendable to P-gp substrates. In contrast, the relationship between the permeability and FaFg of the CYP3A substrate and P-gp & CYP3A substrate drugs could not be explained by this regression curve, and the FaFg values estimated using this regression curve were overestimated (Method 1). This is because the regression curve of permeability and FaFg should change depending on the Fg of each drug[24]. Therefore, we attempted to estimate the FaFg of CYP3A and CYP3A & P-gp substrate drugs using Eq. (21) derived from theoretical considerations and permeabilities with and without the CYP inhibitor (Method 2). However, the FaFg was underestimated by this method in contrast to that by Method 1. We speculated that the CYP3A activity in this monolayer model was higher than that in in vivo enterocytes. Therefore, we used the ratio of CYP3A expression in the monolayer model to that in primary enterocytes as a parameter to account for the differences in the CYP3A activity between the in vitro and in vivo conditions (Method 3). When using Method 3, the estimated FaFg values of seven of nine drugs including CYP3A, P-gp, and CYP3A & P-gp substrates were within 1.5 times. This would be the first example incorporating quantitative differences in metabolic enzyme activity (expression level) between in vitro and in vivo systems when estimating in vivo absorption. Thus, M&S is a valuable tool for quantitatively interpreting the results of experiments using organoids with multiple functions. The FaFg of rifabutin was overestimated by all estimation methods, and its Fg was also overestimated by a previous prediction method[49], possibly because of the influence of gastrointestinal metabolic enzymes other than CYP3A on the Fg value. For example, rifabutin is deacetylated by human arylacetamide deacetylase expressed in the human intestine[50,51]. It is possible that this influence was not considered in previous investigations and in the in vitro permeability test performed in this study.

Our monolayer model exhibited reproducible tolerability against FaSSIF buffer. Generally, aqueous phosphate buffers are used as donor buffers; however, the use of FaSSIF can more accurately predict human drug absorption[52]. New modalities outside the scope of Lipinski's "role of five" have been employed to develop high-molecular-weight and lipophilic compounds, represented by cell-permeable cyclic peptides and proteolysis-targeting chimeras (PROTAC)[53–55]. With the increasing use of these new modalities, the ability to use artificial bile juice, which can solubilize candidate drugs and reduce the adsorption of these compounds against labware, can be a crucial factor in assessing their absorption. Our model can be considered superior due to its adaptability in assessing these new modalities.

Despite scientific and technological advances in recent years, the success rate of new drug discovery remains low[56,57]. One of the reasons for this is the increased complexity of drug molecular structures and modes of action, making prediction of their action in humans increasingly challenging. We hope that integrating the evaluation from the developed model can aid in selecting compounds with good absorption and accurately predicting their absorption in humans, thereby contributing to increased success rate in clinical trials.

Materials and methods

Primary human enterocytes

Cryopreserved primary duodenal enterocytes were purchased from In Vitro ADMET Laboratories (Lot No. HE3052 (primary enterocyte1) and HE3071 (primary enterocyte2)). For the RNA extraction, these cells were thawed according to the manufacturer's protocol and TRIzol was immediately added. Detailed RNA extraction protocol was referred to in the section on quantitative RT-PCR.

Isolation of human duodenal crypts and generation and maintenance of organoids

Human duodenal tissues were obtained from patients undergoing pancreaticoduodenectomy at Hokuto Hospital. The patients provided written informed consent, and the study was approved by the ethical committees of Hokuto Hospital (Reference number: 1050) and Chugai Pharmaceutical Co., Ltd. (Reference number: E19028

and E19078). Crypt isolation from duodenal tissue and generation of organoids were performed according to a previous report[13]. The organoid establishment medium consisted of advanced DMEM/F-12, antimycotic antibiotic solution (Thermo Fisher Scientific), primocin (Thermo Fisher Scientific), 10 mM HEPES (Thermo Fisher Scientific), 2 mM GlutaMAX-I (Thermo Fisher Scientific), and supplemented with 1 × B-27 supplement (Thermo Fisher Scientific), 2 × N-2 supplement (Thermo Fisher Scientific), 1.25 mM *N*-acetylcysteine, 10 nM gastrin (3006; Tocris), 10 mM nicotinamide (Sigma), 10% Afamin/Wnt3a CM (J2-001; JSR)[59] or 50 ng/mL recombinant human Wnt3a (5036-WN-010; R&D systems), 1 µg/mL recombinant human R-spondin-1 (120–38; PeproTech), 100 ng/mL animal-free recombinant human EGF (AF-100–15; PeproTech), 100 ng/mL recombinant human noggin (120-10C; PeproTech), 500 nM A83-01 (2939; Tocris), 10 µM SB202190 (S7067; Sigma), 1 µM prostaglandin E2 (P0409; Sigma), 100 ng/mL recombinant human FGF-10 (100–26; PeproTech), 1 ng/mL recombinant human FGF-basic (100-18B; PeproTech), and 10.5 µM Y-27632 (Y0503; Sigma). IntestiCult™ Organoid Growth Medium (Human) (06,010; STEMCELL Technologies) was utilized for organoid maintenance culture. The organoids were passaged once a week in Gentle Cell Dissociation Reagent (GCDR) (100–0485; STEMCELL Technologies) based on the protocol of STEMCELL Technologies. Briefly, the medium was removed, and 1 mL GCDR was added on the top of the exposed dome in each well and incubated for 1 min. The Matrigel dome was disrupted by pipetting, and samples were collected in 15 mL STEMFULL™ tubes (MS-90150; Sumitomo Bakelite). The collected organoids were incubated at room temperature with rotating (~ 40 rpm) for 10 min and centrifuged at 290 × *g* for 5 min at 4 °C. The supernatant was discarded, and 3 mL of ice-cold DMEM/F-12 + 1% BSA was added to a conical tube and pipetted up and down vigorously approximately 15 times to generate organoid fragments. After another centrifugation at 200 × *g* for 5 min at 4 °C, these fragments were resuspended in a Matrigel (356,231; Corning) mixture diluted to 50% with ice-cold DMEM/F-12 + 1% BSA, and 50 µL of this solution was seeded onto 24 well cell culture plates and solidified in a 37 °C CO_2 incubator. After gel formation, 750 µL culture medium was added to each well, and the culture plate was incubated at 37 °C and 5% CO_2. The medium was changed every 2–3 days. Organoids from passage 8 to passage 24 were used for the experiments.

ECM coating

A Transwell 0.4 µm pore polyester membrane insert with 24 wells (Corning, 3470 and 3378) was coated with 100 µL of ECM solution at 37 °C and 5% CO_2 for at least 2 h. Matrigel Growth factor reduced (356,231; Corning) was diluted 50-fold with ice-cold PBS (−) for Matrigel coating; rat tail collagen I (A1048301; Thermo Fisher Scientific) was diluted to 16.5 µg/mL with 20 mM acetic acid for Col-I coating; fibronectin bovine plasma (F1141; Sigma) was diluted 20-fold with ice-cold PBS (−) for fibronectin coating; Col-IV (C6745; Sigma) was diluted tenfold with ice-cold HBSS for Col-IV coating; and easy iMatrix-511 silk (892,024; Nippi) was directly utilized for iMatirx-511 coating.

Cell seeding for transwell

Human duodenal organoids maintained using IntestiCult™ for 7 days were collected using GCDR. The collected organoids were incubated at room temperature with rotation (~ 40 rpm) for 10 min and centrifuged at 290 × *g* for 5 min at 4 °C. The supernatant was discarded, and 3 mL of ice-cold DMEM/F12 was added to a conical tube and pipetted up and down approximately 15 times to generate organoid fragments. After centrifugation at 200 × *g* for 5 min at 4 °C and the removal of supernatant, 2 mL of 2.5 × TrypLE Select solution (mixture of TrypLE select (10 ×) (Thermo Fisher Scientific):PBS (−) = 1:3) was added to the conical tube, and organoid fragments were digested into single cells in a 37 °C water bath for 5–10 min. Then, 2 mL of basal medium was added to each conical tube, and the mixture was well-pipetted and passed through a 70 µm cell strainer. Cells were centrifuged at 290 × *g* for 5 min at 4 °C. If the cells did not pellet, additional centrifugation was performed at ~ 400 × *g* for 3 min at 4 °C. After removing the supernatant, the expansion medium was added to the conical tube and cell counting was performed. The cell count was adjusted to 5.0×10^5 cells/mL and seeded into Transwell (1.0×10^5 cells/well, 200 µL). Next, 800 µL of expansion medium was added to the basal side of Transwell, and cells were cultured at 37 °C and 5% CO_2. To select digestion enzymes, 0.05% Trypsin/EDTA solution (32,778–34; Nacalai Tesque) was also utilized instead of TrypLE Select solution and the results were compared.

Preparation of expansion and differentiation medium from the first to the third step

Basal medium was prepared using Advanced DMEM/F-12 supplemented with 10 mM HEPES, 2 mM GlutaMAX-I, and penicillin–streptomycin (Thermo Fisher Scientific). To prepare the expansion medium, IntestiCult Organoid Growth Medium supplemented with 10 µM Y-27632 was utilized as medium 1. A basal medium supplemented with 1 × B-27 Supplement, 2 × N-2 Supplement, 1 mM *N*-acetylcysteine, 10 nM [Leu15]-Gastrin I human (G9145; Sigma), 20% Afamin/Wnt3a CM, 50 ng/mL mouse EGF recombinant protein (PMG8041; Thermo Fisher Scientific), 100 ng/mL recombinant murine Noggin (250–38; PeproTech), 1 µg/mL recombinant human R-spondin-1, 500 nM A83-01, and 10 µM Y-27632 (034–24,024; FUJIFILM Wako Chemicals) was utilized as Medium 2. Medium 3 was prepared by adding Medium 2 to 10 mM nicotinamide (N0636; Sigma) and 10 µM SB202190. Medium 4 was prepared by adding Medium 3 to 10 nM prostaglandin E2. Medium 5 was prepared by adding Medium 3 to 10 µM CHIR-99021 (S2924; Selleck) only for the first 2 days. Medium 6 (WENRAYg + IF) was prepared using a basal medium supplemented with 1 × B-27 supplement, 1 mM *N*-acetylcysteine, 10 nM [Leu15]-gastrin I human, 20% Afamin/Wnt3a CM, 50 ng/mL mouse EGF recombinant protein, 100 ng/mL recombinant murine noggin, 1 µg/mL recombinant human R-spondin-1, 500 nM A83-01, 100 ng/mL recombinant human IGF-I (590,906; BioLegend), 50 ng/mL human heat stable bFGF recombinant protein (PHG0369; Thermo Fisher Scientific), and 10 µM Y-27632. The expansion medium was changed every 2–3 days.

To prepare the differentiation medium, NAg medium was prepared using the basal medium supplemented with 1 × B-27 supplement, 1 mM *N*-acetylcysteine, 10 nM [Leu15]-Gastrin I human, 100 ng/mL recombinant murine noggin, and 500 nM A83-01. The ENAg medium was prepared by adding NAg medium to 50 ng/mL mouse EGF recombinant protein. The ENAg + N_2 medium was prepared by adding ENAg medium to 2 × N-2 supplement. ENAIFg medium was prepared by adding ENAg medium to 100 ng/mL recombinant human IGF-I and 50 ng/mL human heat stable bFGF recombinant protein.

Preparation of expansion and differentiation media after the fourth step

Medium 6 (WENRAYg + IF) and the ENAg medium were supplemented with various lipid mixtures. AlbuMAX I Lipid-Rich BSA (11,020–039; Thermo Fisher Scientific) was dissolved in DMEM/F-12 to prepare a solution with a 40 mg/mL concentration. Similarly, a BSA solution was also prepared (A7030; Sigma). These solutions were then passed through a 0.22 μm filter and were added to the expansion and differentiation medium to achieve a final concentration of 10% (4 mg/mL). Palmitic acid (P5585; Sigma), palmitoleic acid (P9417; Sigma), stearic acid (199–10,995; FUJIFILM Wako Chemicals), oleic acid (O1008; Sigma), linoleic acid (L1012; Sigma), and a-linolenic acid (L2376; Sigma) were added to the expansion medium and differentiation medium to give a final concentration of 50 μM. GW501516 (SML1491; Sigma) was utilized at concentrations of 1 μM and 10 μM, TAK-875 (S2637; Selleck) was utilized at concentrations of 0.1 μM and 1 μM. Furthermore, 5 μg/mL lysophosphatidylcholine (123–03,781; FUJIFILM Wako Chemicals), 5 μg/mL phosphatidylcholine (163–21,181; FUJIFILM Wako Chemicals), and 1 μM cholesterol (034–03,002; FUJIFILM Wako Chemicals) were used as additional lipids. To induce the expression of absorption-related genes, during the last 2 days of the differentiation protocol, the differentiation medium was supplemented with 100 nM VD3 (D1530; Sigma) and/or 10 μM rifampicin (189–01001; FUJIFILM Wako Chemicals). The final culture conditions optimized in this study were Medium 6 containing 4 mg/mL AlbuMAX for 4 days and ENAg medium containing 4 mg/mL AlbuMAX for 6 days (containing 100 nM VD3 for the last 2 days), for a total of 10 days.

Measurement of TEER value

The integrity of the monolayer was evaluated using the TEER. The TEER value was measured using a Millicell ERS-2 system (Merck) and calculated according to the manufacturer's instructions.

MTT staining assay of monolayer culture

Viable cells in the monolayer culture were subjected to MTT staining assay. MTT (23,547–76; Nacalai Tesque) was dissolved in D-PBS (−) to create a 5 mg/mL solution. This solution was passed through a 0.22 μm filter and diluted tenfold with basal medium to prepare the MTT solution, and the monolayer culture was incubated with MTT solution at 37 °C and 5% CO_2 for approximately 30 min to yield purple formazan crystals. After the monolayer culture was stained, bright-field images were obtained using an inverted microscope (IX83; Olympus).

Quantitative RT-PCR

Total RNA was extracted from organoids and monolayer culture using TRIzol and purified using the RNeasy mini kit (74,104; QIAGEN). Total RNA concentration and purity were determined using NanoDrop™ (Thermo Fisher Scientific). cDNA was synthesized using the Superscript III First-strand synthesis system for RT-PCR (18,080–051; Thermo Fisher Scientific). Quantitative RT-PCR was conducted in duplicate for each gene on the StepOnePlus Real-Time PCR System (Thermo Fisher Scientific) using TaqMan™ fast advanced master mix for qPCR (4,444,557; Thermo Fisher Scientific) and a TaqMan™ gene expression assay (FAM) (4,331,182; Thermo Fisher Scientific). The reaction was performed at 95 °C for 20 s with 40 cycles of 95 °C for 1 s and 60 °C for 20 s (Fast mode). The TaqMan primers and probes utilized in this study are listed in the Supplementary table 1.

RNA sequencing and heatmap analysis

The quality of the total RNA was evaluated using a TapeStation or BioAnalyzer (Agilent Technologies), followed by the amplification of double-strand cDNA using SMART-Seq® v4 Ultra® Low Input RNA Kit for Sequencing (Takara Bio) and Nextera XT DNA Library Preparation Kit (Illumina) and Nextera XT Index Kit v2 (Illumina) to prepare sequencing libraries. The libraries were sequenced using NovaSeq 6000 (Illumina). The RNA sequencing reads were mapped to GRCh38 with RefSeq transcript annotation using bowtie (version 1.1.2), and the fragments per kilobase of exon per million mapped fragments (FPKM) were calculated using RSEM (v1.2.31; The GNU General Public License). The conversion from PFKM to transcripts per million (TPM) and calculation of $\log_2$ (TPM + 1) were conducted using R version 4.2.3 (R Foundation for Statistical Computing). Heatmap analysis was performed using ComplexHeatmap package (version 2.14.0).

CYP3A activity assay

The P450-Glo™ CYP3A4 Luciferin-IPA assay (V9001; Promega) was performed to assess CYP3A activity according to the manufacture's instruction. The apical and basal sides of the monolayer culture were washed with basal medium. Next, 100 μL of the basal medium containing 3 μM Luciferin-IPA was added into apical side, and the Transwell was incubated at 37 °C and 5% CO_2 for 60 min. Luminescence was measured using EnSpire (PerkinElmer).

EdU uptake assay

EdU staining was performed using the Click-iT Plus EdU cell proliferation kit for imaging and Alexa Fluor 555 dye (C10638; Thermo Fisher Scientific) according to the manufacturer's instruction. EdU-positive cells were

observed using a confocal microscope (A1; Nikon) with z-step series, and the image was analyzed using NIS elements (Nikon).

Immunofluorescence analysis

After removing the culture medium, the monolayer was fixed using 4% paraformaldehyde for 15 min at room temperature. After washing with D-PBS (−), BlockAid Blocking Solution (B10710; Thermo Fisher Scientific) containing 0.5% Triton X-100 was added and incubated for 1 h at room temperature. The monolayer was incubated with primary antibodies [anti-ZO-1 antibody Alexa Fluor 488 (MA3-39,100-A488; Thermo Fisher Scientific), anti-E-cadherin antibody (PA5-32,178; Thermo Fisher Scientific), and anti-MUC2 antibody (NBP2-25,221; Novus Biologicals)] in blocking solution containing 0.3% Triton X-100 at 4 °C overnight. After washing with PBS three times, the monolayer was incubated overnight at 4 °C with secondary antibodies [goat anti-mouse IgG (H + L) highly cross-adsorbed secondary antibody Alexa Fluor Plus 488 (A32723; Thermo Fisher Scientific), goat anti-rabbit IgG (H + L) highly cross-adsorbed secondary antibody Alexa Fluor Plus 555 (A32732; Thermo Fisher Scientific)] in blocking solution containing 0.3% Triton X-100. After washing two times, the nucleus and F-actin were stained with D-PBS (−) containing 1 µg/mL 4′,6-diamidino-2-phenylindole, dihydrochloride (DAPI, D1306; Thermo Fisher Scientific) and 3 U/mL DyLight 650 Phalloidin (12956S; Cell Signaling Technology) for 1 h at room temperature. Fluorescence was analyzed using a confocal microscope (A1; Nikon) with z-step series, and the image was analyzed using NIS elements (Nikon).

Transmission electron microscopy

The monolayer culture was fixed with 1.5% paraformaldehyde and 0.5% glutaraldehyde in D-PBS (−) at 4 °C for 24 h. After washing with D-PBS (−), the culture was further fixed using 1% osmium. The fixed organoids were dehydrated by washing them in a graded series of ethanol solutions, followed by incubation with propylene oxide, and embedding in epoxy resin. The resin was heat-polymerized and ultrathin sections were prepared using an ultramicrotome. These sections were double-stained with uranyl acetate and lead citrate and observed using a transmission electron microscope (JEM-1400; JEOL).

FaSSIF tolerability assay

The FaSSIF buffer (pH 6.5) was prepared according to the manufacturer's instructions using FaSSIF/FeSSIF/FaSSGF powder (FFF02; Biorelevant). FaSSIF buffer (pH 6.5) containing 200 µM lucifer yellow (L0144; Sigma) was added to the apical side of the Transwell®, and the transporter buffer consisting of 10 mM HEPES and 4% (w/v) BSA in HBSS (pH 7.4) was added to the basal side of the Transwell. After 2 h of incubation, the concentration of lucifer yellow on the basal side was determined by a fluorescent signal measured with EnSpire using 428 nm excitation and 536 nm emission filters. The apparent permeability coefficient (P_{app}) was calculated according to the following equation:

$$P_{app} = \frac{dQ}{dt} \times \frac{1}{A \times C_0} \tag{1}$$

where dQ/dt represents the compound transported to the basal or apical side per unit time, A is the surface area of the cell culture insert, and C_0 is the initial concentration of the compound.

Efflux drug transporter assay

For the digoxin efflux assay, the apical and basal sides of monolayer cultures were washed using efflux assay buffer consisting of 10 mM HEPES and 1% (w/v) BSA in HBSS (pH 7.4). Next, an efflux assay buffer containing 200 µM lucifer yellow, 10 µM digoxin (D6003; Sigma), with or without 10 µM zosuquidar (SML1044; Sigma), a P-gp inhibitor, was added to the apical or basal side of monolayer cultures, and efflux assay buffer with or without 10 µM zosuquidar was added to the basal or apical side of monolayer cultures. The concentration of digoxin in the efflux assay buffer was determined using LC–MS/MS analysis. For the sulfasalazine efflux assay, 10 µM sulfasalazine (S0580; Tokyo Chemical Industry) was utilized as a substrate and 5 µM Ko143 (K2144; Sigma) was utilized as a BCRP inhibitor. P_{app} was calculated using the Eq. (1).

Midazolam permeability and metabolizing assay

Prior to the assay, the apical side of the monolayer cultures was washed with FaSSIF buffer (pH 6.5), and the basal side with the transporter buffer. FaSSIF buffer (pH 6.5) containing 0.2, 2 or 5 µM midazolam (135–13,791; FUJIFILM Wako Chemicals) in the presence or absence of 1 mM ABT (A3940; Sigma) was added to the apical side of the monolayer cultures, and the transporter buffer, in the presence or absence of 1 mM ABT, was added to the basal side of the monolayer cultures The concentrations of midazolam, 1′-OH midazolam, and 4-OH midazolam were determined using LC–MS/MS analysis. The value of P_{app} was calculated using the Eq. (1).

Raloxifene permeability and metabolizing assay

Prior to the assay, the apical side of the monolayer cultures was washed with FaSSIF buffer (pH 6.5), and the basal side with the transporter buffer. FaSSIF buffer (pH 6.5) containing 5 µM raloxifene (R0109; Tokyo Chemical Industry) was added to the apical side of the monolayer cultures, and the transporter buffer was added to the basal side of the monolayer cultures. The concentrations of raloxifene, raloxifene 6-glucuronide, and raloxifene 4′-glucuronide were determined using LC–MS/MS analysis.

Irinotecan metabolizing assay

Prior to the assay, the apical side of the monolayer cultures was washed with FaSSIF buffer (pH 6.5), and the basal side with the transporter buffer. FaSSIF buffer (pH 6.5) containing 10 μM irinotecan (I1406; Sigma) in the presence or absence of 20 μM loperamide (L4762; Sigma) was added to the apical side of the monolayer cultures, and the transporter buffer was added to the basal side of the monolayer cultures. After 3 h, the apical and basal buffers were discarded, and 100 μL of 80% (v/v) acetonitrile in water was added to the apical side and incubated for 10 min to extract the cell compartments. The concentration of SN-38, an irinotecan metabolite, was determined by LC–MS/MS analysis.

Permeability assays for commercially available drugs

Prior to the assay, the apical side of the monolayer cultures was washed with FaSSIF buffer (pH6.5), and the basal side with the transporter buffer. Permeability assays for 19 commercially available drugs were conducted using cocktail substrates. Cocktail 1 consisted of metoprolol (M5391; Sigma), enalaprilat (E1302; Tokyo Chemical Industry), nadolol (N1892; Sigma), atenolol (A7655; Sigma), and antipyrine (A5882; Sigma); Cocktail 2 consisted of ketoprofen (K1751; Sigma), propranolol (163–24,501; FUJIFILM Wako Chemicals), losartan (550–70,081; FUJIFILM Wako Chemicals), ranitidine (R101; Sigma), and acyclovir (019–17,421; FUJIFILM Wako Chemicals); Cocktail 3 consisted of rosiglitazone (180–02,653; FUJIFILM Wako Chemicals), carbamazepine (034–23,701; FUJIFILM Wako Chemicals), famotidine (066–06,701; FUJIFILM Wako Chemicals), and amiloride (A2599; Tokyo Chemical Industry), oxacillin (154–02,131; FUJIFILM Wako Chemicals); and Cocktail 4 consisted of glimepiride (071–05,691; FUJIFILM Wako Chemicals), pitavastatin (169–24,863; FUJIFILM Wako Chemicals), theophylline (209–09,932; FUJIFILM Wako Chemicals), and furosemide (F4381; Sigma), all at a concentration of 10 μM. FaSSIF buffer (pH 6.5) containing either cocktail 1, cocktail 2, cocktail 3, or cocktail 4 substrates was added to the apical side of the monolayer cultures, and the transporter buffer was added to the basal side of the monolayer cultures. For the donor comparison permeability assay, FaSSIF buffer (pH 6.5) containing 3 μM digoxin with or without 10 μM zosuquidar was added to the apical side of the monolayer cultures, and the transporter buffer with or without 10 μM zosuquidar was added to basal side of the monolayer cultures. FaSSIF buffer (pH 6.5) containing 10 μM sulfasalazine with or without 5 μM Ko143 was added to the apical side of the monolayer cultures, and the transporter buffer with or without 5 μM Ko143 was added to basal side of the monolayer cultures. For the permeability assay of CYP3A substrates, FaSSIF buffer (pH 6.5) containing 2 μM of each substrate with or without 1 mM ABT (CYP3A substrate; midazolam, rifabutin (R0211; Tokyo Chemical Industry), nifedipine (N7634; Sigma), felodipine (F0814; Tokyo Chemical Industry), alprazolam (016–17,171; FUJIFILM Wako Chemicals), and sildenafil (S0986; Tokyo Chemical Industry)) was used. For the permeability assay of P-gp & CYP3A substrates, FaSSIF buffer (pH 6.5) containing 5 μM of each substrate with or without 1 mM ABT (P-gp & CYP3A substrates: cyclosporine (031–24,931, FUJIFILM Wako Chemicals) and tacrolimus (063–06,071, FUJIFILM Wako Chemicals)) was used. The concentration of these substrates was determined by LC–MS/MS analysis. P_{app} was calculated using Eq. (1).

LC–MS/MS analysis

The concentration of compounds was determined by LC–MS/MS using the Ultra High Performance Liquid Chromatograph (UPLC) system Nexera (Shimadzu) and QTRAP5500 (SCIEX) or QTRAP6500 (SCIEX). The collected supernatant was mixed with acetonitrile, methanol, or a 1:1 mixture of acetonitrile and methanol containing internal standards. These mixtures were centrifuged at 15,000 rpm for 15 min at 4 °C or filtered using a MultiScreen Solvinert 96 Well Filter Plate (MSRLN0450, Merck). The supernatant was analyzed using LC–MS/MS. The columns utilized for LC–MS/MS analysis were ACQUITY UPLC BEH C18 Column (1.7 μm, 2.1 mm × 50 mm, Waters) for Digoxin, XBridge BEH C18 (3.5 μm, 2.1 mm × 100 mm, Waters) for midazolam, 1′-OH midazolam, and 4-OH midazolam, ACQUITY UPLC BEH C18 Column (1.7 μm, 2.1 mm × 100 mm, Waters) for raloxifene, raloxifene 6-glucronide, and raloxifene 4′-glucronide, CAPCELL PAK ADME-HR S3 (3.0 μm, 2.1 mm × 100 mm, OSAKA SODA) for sulfasalazine, L-column3 C18 (2.0 μm, 2.0 mm × 50 mm, Chemicals Evaluation and Research Institute) for SN-38, XSelect CSH C18 (3.5 μm, 2.1 mm × 50 mm, Waters) for cocktail 1, cocktail 3, and cocktail 4 substrates, CORTECS C18 + (2.7 μm, 2.1 mm × 50 mm, Waters) for cocktail 2 substrates, and Ascentis Express C18 (2.7 μm, 2.1 mm × 50 mm, Merck) for alprazolam, felodipine, nifedipine, rifabutin, sildenafil, and tacrolimus, XSelect Peptide CSH C18 XP Column (2.5 μm, 2.1 mm × 50 mm, Waters) for cyclosporine. The detailed conditions are listed in Supplementary Table 2.

Mathematical modeling of in vitro *permeability test*

We determined drug permeability by performing an in vitro permeability test using the three-compartment model shown in Fig. 8a. Under steady state conditions, the control apparent permeability ($P_{app,Control}$) and that with 1 mM ABT, a pan-CYP inhibitor, ($P_{app,Control}$) were calculated using the following equations:

$$P_{app,Control} = \frac{P_1 \times P_3}{P_2 + P_3 + CL/S_{met,vitro}} \tag{2}$$

$$P_{app,Inh} = \frac{P_1 \times P_3}{P_2 + P_3} \tag{3}$$

where P_1, P_2, P_3, and $CL/S_{met,vitro}$ represent the intrinsic permeation clearance per surface area in the apical-to-cell direction, intrinsic permeation clearance per surface area in the cell-to-apical direction, intrinsic permeation clearance per surface area in the cell-to-basal direction, and intrinsic metabolic clearance per surface area mediated by CYP3A, respectively. By transforming Eqs. (2) and (3), the following equations can be obtained:

$$\frac{P_{app,Inh}}{P_{app,Control}} = 1 + \frac{CL/S_{met,vitro}}{P_2 + P_3} \tag{4}$$

$$\frac{1}{P_{app,Control}} - \frac{1}{P_{app,Inh}} = \frac{CL/S_{met,vitro}}{P_1 \times P_3} \tag{5}$$

Mathematical modeling of in vivo absorption

We described the in vivo drug absorption through the three-compartment model shown in Fig. 8b. We assumed a well-stirred model to drug concentration in the luminal side (C_{lum}). The C_{lum} and drug concentration in the enterocyte were determined by the following ordinary differential equations (ODEs):

$$V_{lum}\frac{dC_{lum}}{dt} = Q\left(C_{in} - C_{lum}\right) + PS_2 \times C_{ent} - PS_1 \times C_{lum} \tag{6}$$

$$V_{ent}\frac{dC_{ent}}{dt} = PS_1 \times C_{lum} - (PS_2 + PS_3 + CL_{met,vivo})C_{ent} \tag{7}$$

where C_{in} represents the drug concentration in the flow to the luminal side, Q, PS_1, PS_2, PS_3, and $CL_{met,vivo}$ represent the flow rate at the luminal side, the intrinsic permeation clearance in the luminal-to-enterocyte direction, the intrinsic permeation clearance in the enterocyte-to-luminal direction, the intrinsic permeation clearance in the enterocyte-to-portal vein direction, and the intrinsic metabolic clearance mediated by CYP3A, respectively. When assuming steady state conditions, these ODEs are transformed as follows:

$$0 = Q\left(C_{in} - C_{lum}\right) + PS_2 \times C_{ent} - PS_1 \times C_{lum} \tag{8}$$

$$0 = PS_1 \times C_{lum} - (PS_2 + PS_3 + CL_{met,vivo})C_{ent} \tag{9}$$

Transforming Eqs. (8) and (9), the following equations can be obtained:

$$\frac{C_{ent}}{C_{in}} = \frac{Q \times PS_1}{Q\left(PS_2 + PS_3 + CL_{met,vivo}\right) + PS_1(PS_3 + CL_{met,vivo})} \tag{10}$$

Intestinal bioavailability (FaFg) was defined as follows:

$$FaFg = \frac{PS_3 C_{ent}}{QC_{in}} \tag{11}$$

Using Eqs. (10) and (11), FaFg was calculated as follows:

$$FaFg = \frac{PS_1 \times PS_3}{Q\left(PS_2 + PS_3 + CL_{met,vivo}\right) + PS_1(PS_3 + CL_{met,vivo})} \tag{12}$$

Extrapolation from in vitro P_{app} to in vivo FaFg

To extrapolate the in vitro drug permeability to the in vivo absorption rate, we made some assumptions:

$$P_2 = P_3 \tag{13}$$

$$\frac{PS_1}{P_1} = \frac{PS_2}{P_2} = \frac{PS_3}{P_3} = S \tag{14}$$

$$\frac{CL_{met,vivo}}{CL/S_{met,vitro}} = S \times SF_{CYP3A} \tag{15}$$

where S and SF_{CYP3A} represent the surface area of the in vivo enterocyte and scaling factor for CYP3A activity bridging in vitro and in vivo, respectively. In this study, SF_{CYP3A} was calculated from the CYP3A4 mRNA expression ratio between the monolayer model and commercially available primary enterocyte. Using Eqs. (4) and (13), the following equations were obtained:

$$\frac{P_{app,Inh}}{P_{app,Control}} = 1 + \frac{CL/S_{met,vitro}}{2 \times P_3} \tag{16}$$

$$\frac{CL/S_{met,vitro}}{P_3} = 2\left(\frac{P_{app,Inh}}{P_{app,Control}} - 1\right) \tag{17}$$

Using Eqs. (3), (5), (12), (14), (15) and (17), the following equations were obtained:

$$FaFg = \frac{P_1 \times P_3}{\frac{Q}{S}\left(P_2 + P_3 + \frac{CL_{met,vivo}}{S}\right) + P_1\left(P_3 + \frac{CL_{met,vivo}}{S}\right)} \tag{18}$$

$$FaFg = \frac{1}{\frac{Q}{S}\left(\frac{P_2+P_3}{P_1\times P_3} + \frac{SF_{CYP3A}\times CL/S_{met,vitro}}{P_1\times P_3}\right) + \left(1 + \frac{SF_{CYP3A}\times CL/S_{met,vitro}}{P_3}\right)} \quad (19)$$

$$FaFg = \frac{1}{\frac{Q}{S}\left(\frac{1}{P_{app,Inh}} + SF_{CYP3A}\left(\frac{1}{P_{app,Control}} - \frac{1}{P_{app,Inh}}\right)\right) + \left(1 + SF_{CYP3A}\times 2\left(\frac{P_{app,Inh}}{P_{app,Control}} - 1\right)\right)} \quad (20)$$

Equation (20) is the FaFg calculation method which is considering the difference in the CYP3A activity between the monolayer model and in vivo enterocytes (Method 3). When assuming that the in vitro CYP3A activity is equal to that in vivo ($SF_{CYP3A} = 1$), Eq. (20) can be transformed as follows:

$$FaFg = \frac{1}{\frac{Q}{S}\times\frac{1}{P_{app,Control}} + 2\frac{P_{app,Inh}}{P_{app,Control}} - 1} \quad (21)$$

Equation (21) is the FaFg calculation method which is considering the effects of CYP3A using the permeability data with and without ABT (Method 2). When the drug is not a substrate of a metabolic enzyme both in vitro and in vivo, it means we can assume that $P_{app,inh}$ is equal to $P_{app,Control}$, Eq. (21) can be transformed as follows:

$$FaFg = Fa = \frac{1}{\frac{Q}{S}\times\frac{1}{P_{app,Control}} + 1} \quad (22)$$

Equation (22) is the FaFg calculation method by the permeability-Fa regression curve of 19 launched drugs (Method 1).

Quantification and statistical analysis

Unless mentioned otherwise, data are presented as the means ± SD of biological replicates, and the number of samples (n) is indicated in Figure legends. Unpaired two-tailed Student's *t*-test was used for the statistical comparison of two groups, and one-way ANOVA, followed by Tukey's or Dunnett's multiple comparison test, was used for the statistical comparison of multiple groups. Detailed information is provided in the Fig. legends. Statistical calculations were performed using GraphPad Prism 7.04 (GraphPad Software). $^{*}P<0.05$; $^{**}P<0.01$; $^{***}P<0.001$; $^{****}P<0.0001$.

Data availability

All data generated or analyzed during this study are included in this published article or supplementary information. The RNA sequencing results are available upon request from the corresponding author due to ethical concerns.

Received: 21 January 2025; Accepted: 24 March 2025
Published online: 03 April 2025

References

1. Zanger, U. M. & Schwab, M. Cytochrome P450 enzymes in drug metabolism: Regulation of gene expression, enzyme activities, and impact of genetic variation. *Pharmacol. Ther.* **138**, 103–141 (2013).
2. Price, E. et al. Global analysis of models for predicting human absorption: QSAR, in vitro, and preclinical models. *J. Med. Chem.* **64**, 9389–9403 (2021).
3. Peters, S. A., Jones, C. R., Ungell, A. L. & Hatley, O. J. Predicting drug extraction in the human gut wall: Assessing contributions from drug metabolizing enzymes and transporter proteins using preclinical models. *Clin. Pharmacokinet.* **55**, 673–696 (2016).
4. Hubatsch, I., Ragnarsson, E. G. E. & Artursson, P. Determination of drug permeability and prediction of drug absorption in Caco-2 monolayers. *Nat. Protoc.* **2**, 2111–2119 (2007).
5. Kus, M., Ibragimow, I. & Piotrowska-Kempisty, H. Caco-2 cell line standardization with pharmaceutical requirements and in vitro model suitability for permeability assays. *Pharmaceutics* **15**, 2523 (2023).
6. Sun, H., Chow, E. C., Liu, S., Du, Y. & Pang, K. S. The Caco-2 cell monolayer: Usefulness and limitations. *Expert Opin. Drug Metab. Toxicol.* **4**, 395–411 (2008).
7. Kwon, O. et al. The development of a functional human small intestinal epithelium model for drug absorption. *Sci. Adv.* **7**(23), eabh1586 (2021).
8. Leo, S. et al. The effect of vitamin D3 and valproic acid on the maturation of human-induced pluripotent stem cell-derived enterocyte-like cells. *Stem Cells* **41**, 775–791 (2023).
9. Inui, T. et al. Functional intestinal monolayers from organoids derived from human iPS cells for drug discovery research. *Stem Cell Res. Ther.* **15**, 57 (2024).
10. Shirai, K. et al. Air-liquid interface culture and modified culture medium promote the differentiation of human induced pluripotent stem cells into intestinal epithelial cells. *Drug Metab. Pharmacokinet.* **55**, 100994 (2024).
11. Clevers, H. Modeling development and disease with organoids. *Cell* **165**, 1586–1597 (2016).
12. Sato, T. et al. Single Lgr5 stem cells build crypt-villus structures in vitro without a mesenchymal niche. *Nature* **459**, 262–265 (2009).
13. Sato, T. et al. Long-term expansion of epithelial organoids from human colon, adenoma, adenocarcinoma, and Barrett's epithelium. *Gastroenterology* **141**, 1762–1772 (2011).
14. Jung, P. et al. Isolation and in vitro expansion of human colonic stem cells. *Nat. Med.* **17**, 1225–1227 (2011).
15. Yin, X. et al. Niche-independent high-purity cultures of Lgr5+ intestinal stem cells and their progeny. *Nat. Methods* **11**, 106–112 (2014).
16. Beumer, J. et al. Enteroendocrine cells switch hormone expression along the crypt-to-villus BMP signalling gradient. *Nat. Cell Biol.* **20**, 909–916 (2018).
17. Fujii, M. et al. Human intestinal organoids maintain self-renewal capacity and cellular diversity in niche-inspired culture condition. *Cell Stem Cell* **23**, 787-793.e6 (2018).

18. Kraiczy, J. et al. DNA methylation defines regional identity of human intestinal epithelial organoids and undergoes dynamic changes during development. *Gut* **68**, 49–61 (2019).
19. He, G.-W. et al. Optimized human intestinal organoid model reveals interleukin-22-dependency of paneth cell formation. *Cell Stem Cell* **29**, 1333-1345.e6 (2022).
20. Zeve, D. et al. Robust differentiation of human enteroendocrine cells from intestinal stem cells. *Nat. Commun.* **13**, 261 (2022).
21. Gunasekara, D. B. et al. A monolayer of primary colonic epithelium generated on a scaffold with a gradient of stiffness for drug transport studies. *Anal. Chem.* **90**, 13331–13340 (2018).
22. Madden, L. R. et al. Bioprinted 3D primary human intestinal tissues model aspects of native physiology and ADME/Tox functions. *IScience* **2**, 156–167 (2018).
23. Yamashita, T. et al. Monolayer platform using human biopsy-derived duodenal organoids for pharmaceutical research. *Mol. Ther. Methods Clin. Dev.* **22**, 263–278 (2021).
24. Michiba, K. et al. Usefulness of human jejunal spheroid-derived differentiated intestinal epithelial cells for the prediction of intestinal drug absorption in humans. *Drug Metab. Dispos.* **50**, 204–213 (2022).
25. Kourula, S. et al. Intestinal organoids as an in vitro platform to characterize disposition, metabolism, and safety profile of small molecules. *Eur. J. Pharm. Sci.* **188**, 106481 (2023).
26. Jensen, K. B. & Little, M. H. Organoids are not organs: sources of variation and misinformation in organoid biology. *Stem Cell Rep.* **18**, 1255–1270 (2023).
27. Xie, F., Ding, X. & Zhang, Q. Y. An update on the role of intestinal cytochrome P450 enzymes in drug disposition. *Acta Pharm. Sin. B* **6**, 374–383 (2016).
28. Low, L. A., Mummery, C., Berridge, B. R., Austin, C. P. & Tagle, D. A. Organs-on-chips: Into the next decade. *Nat. Rev. Drug Discov.* **20**, 345–361 (2021).
29. Miyazaki, T. et al. Laminin E8 fragments support efficient adhesion and expansion of dissociated human pluripotent stem cells. *Nat. Commun.* **3**, 1236 (2012).
30. Nishiuchi, R. et al. Ligand-binding specificities of laminin-binding integrins: A comprehensive survey of laminin-integrin interactions using recombinant alpha3beta1, alpha6beta1, alpha7beta1 and alpha6beta4 integrins. *Matrix Biol.* **25**, 189–197 (2006).
31. Miyoshi, H. et al. Prostaglandin E2 promotes intestinal repair through an adaptive cellular response of the epithelium. *EMBO J.* **36**, 5–24 (2017).
32. Kozuka, K. et al. Development and characterization of a human and mouse intestinal epithelial cell monolayer platform. *Stem Cell Rep.* **9**, 1976–1990 (2017).
33. Beumer, J. & Clevers, H. Cell fate specification and differentiation in the adult mammalian intestine. *Nat. Rev. Mol. Cell Biol.* **22**, 39–53 (2021).
34. Miyamoto, J. et al. Nutritional signaling via free fatty acid receptors. *Int. J. Mol. Sci.* **17**, 450 (2016).
35. Fan, J. et al. Up-regulation of transporters and enzymes by the vitamin D receptor ligands, 1alpha,25-dihydroxyvitamin D3 and vitamin D analogs, in the Caco-2 cell monolayer. *J. Pharmacol. Exp. Ther.* **330**, 389–402 (2009).
36. Qin, X. & Wang, X. Role of vitamin D receptor in the regulation of CYP3A gene expression. *Acta Pharm. Sin. B* **9**, 1087–1098 (2019).
37. Jarc, T. et al. Demonstrating suitability of the Caco-2 cell model for BCS-based biowaiver according to the recent FDA and ICH harmonised guidelines. *J. Pharm. Pharmacol.* **71**, 1231–1242 (2019).
38. Zollinger, A. J. & Smith, M. L. Fibronectin, the extracellular glue. *Matrix Biol.* **60–61**, 27–37 (2017).
39. Wang, Y. et al. Bioengineered systems and designer matrices that recapitulate the intestinal stem cell niche. *Cell. Mol. Gastroenterol. Hepatol.* **5**, 440-453.e1 (2018).
40. Tanaka, K. et al. Development of rat duodenal monolayer model with effective barrier function from rat organoids for ADME assay. *Sci. Rep.* **13**, 12130 (2023).
41. Frankland, S. et al. Serum lipoproteins promote efficient presentation of the malaria virulence protein PfEMP1 at the erythrocyte surface. *Eukaryot. Cell* **6**, 1584–1594 (2007).
42. Garcia-Gonzalo, F. R. & Izpisúa Belmonte, J. C. Albumin-associated lipids regulate human embryonic stem cell self-renewal. *PLoS ONE* **3**, e1384 (2008).
43. Nakamura, N. et al. Evaluation of culture time and media in an in vitro testis organ culture system. *Birth Defects Res.* **109**, 465–474 (2017).
44. Vinarov, Z. et al. Impact of gastrointestinal tract variability on oral drug absorption and pharmacokinetics: an UNGAP review. *Eur. J. Pharm. Sci.* **162**, 105812 (2021).
45. Dotti, I. et al. Alterations in the epithelial stem cell compartment could contribute to permanent changes in the mucosa of patients with ulcerative colitis. *Gut* **66**, 2069–2079 (2017).
46. Wolking, S., Schaeffeler, E., Lerche, H., Schwab, M. & Nies, A. T. Impact of genetic polymorphisms of ABCB1 (MDR1, P-glycoprotein) on drug disposition and potential clinical implications: Update of the literature. *Clin. Pharmacokinet.* **54**, 709–735 (2015).
47. Chen, L. & Prasad, G. V. R. CYP3A5 polymorphisms in renal transplant recipients: Influence on tacrolimus treatment. *Pharmgenomics Pers. Med.* **11**, 23–33 (2018).
48. Heyes, N., Kapoor, P. & Kerr, I. D. Polymorphisms of the multidrug pump ABCG2: A systematic review of their effect on protein expression, function, and drug pharmacokinetics. *Drug Metab. Dispos.* **46**, 1886–1899 (2018).
49. Ando, H., Hisaka, A. & Suzuki, H. A new physiologically based pharmacokinetic model for the prediction of gastrointestinal drug absorption: Translocation model. *Drug Metab. Dispos.* **43**, 590–602 (2015).
50. Nakajima, A. et al. Human arylacetamide deacetylase is responsible for deacetylation of rifamycins: Rifampicin, rifabutin, and rifapentine. *Biochem. Pharmacol.* **82**, 1747–1756 (2011).
51. Watanabe, A. et al. Human arylacetamide deacetylase is a principal enzyme in flutamide hydrolysis. *Drug Metab. Dispos.* **37**, 1513–1520 (2009).
52. Wuyts, B. et al. Evaluation of fasted state human intestinal fluid as apical solvent system in the Caco-2 absorption model and comparison with FaSSIF. *Eur. J. Pharm. Sci.* **67**, 126–135 (2015).
53. Shultz, M. D. Two decades under the influence of the rule of five and the changing properties of approved oral drugs. *J. Med. Chem.* **62**, 1701–1714 (2019).
54. Ohta, A. et al. Validation of a new methodology to create oral drugs beyond the rule of 5 for intracellular tough targets. *J. Am. Chem. Soc.* **145**, 24035–24051 (2023).
55. Pike, A., Williamson, B., Harlfinger, S., Martin, S. & McGinnity, D. F. Optimising proteolysis-targeting chimeras (PROTACs) for oral drug delivery: A drug metabolism and pharmacokinetics perspective. *Drug Discov. Today* **25**, 1793–1800 (2020).
56. Dowden, H. & Munro, J. Trends in clinical success rates and therapeutic focus. *Nat. Rev. Drug Discov.* **18**, 495–496 (2019).
57. Sun, D., Gao, W., Hu, H. & Zhou, S. Why 90% of clinical drug development fails and how to improve it?. *Acta Pharm. Sin. B* **12**, 3049–3062 (2022).
58. Varma, M. V. S. et al. Physicochemical space for optimum oral bioavailability: Contribution of human intestinal absorption and first-pass elimination. *J. Med. Chem.* **53**, 1098–1108 (2010).
59. Mihara, E. et al. Active and water-soluble form of lipidated Wnt protein is maintained by a serum glycoprotein afamin/alpha-albumin. *Elife* **5**, e11621 (2016).

Acknowledgements
We acknowledge the patients and their families for their contributions to this study. We also thank K. Nishihara, K. Kuwana, Y. Suzuki, F. Yokoi, K. Tokuda, M. Kamiura, H. Sakumoto, M. Yano, and Y. Kei for their help and support in conducting the experiments. This study was funded by Chugai Pharmaceutical Co., Ltd.

Author contributions
K. Tanaka, S.B., K. Nakano, T. Miyayama, T.Y., H.N., K. Terao, and Y.K. designed research; K. Tanaka., S.B., S.K., K.U., A.K., and T.Y. performed research; K. Tanaka, T. Mochizuki, T.T., and A.K. analyzed data; and K. Tanaka and T. Mochizuki wrote the paper.

Declaration

Competing interests
The authors declare no competing interests.

Ethics approval
All patients provided written informed consent, and the study was approved by the ethical committees of Hokuto Hospital (Reference number: 1050) and Chugai Pharmaceutical Co., Ltd. (Reference number: E19028 and E19078). All methods used were in accordance with the medical code of ethics, the revised declaration of Helsinki, and applicable laws.

Additional information
Supplementary Information The online version contains supplementary material available at https://doi.org/10.1038/s41598-025-95823-z.

Correspondence and requests for materials should be addressed to K.T.

Reprints and permissions information is available at www.nature.com/reprints.

Publisher's note Springer Nature remains neutral with regard to jurisdictional claims in published maps and institutional affiliations.